

Petrogenetic evolution of Late Paleozoic rhyolites of the Harvey Group, southwestern New Brunswick (Canada) hosting uranium mineralization

J. Dostal¹ · T. R. van Hengstum² · J. G. Shellnutt³ · J. J. Hanley¹

Received: 23 February 2016 / Accepted: 26 May 2016 / Published online: 16 June 2016
© Springer-Verlag Berlin Heidelberg 2016

Abstract The 360 Ma subaerial felsic volcanic and volcanoclastic rocks of the Harvey Group form a belt about 15 km long and 3 km wide in southwestern New Brunswick (Canada) that has been correlated with parts of the Mount Pleasant caldera complex, the site of a significant polymetallic (tin, tungsten, molybdenum, indium and bismuth) deposit. The Harvey volcanic rocks are highly fractionated peraluminous within-plate F-rich rhyolites, which host uranium mineralization. The rocks were modified by late-magmatic and post-magmatic processes. A comparison of the composition of whole rocks and melt inclusions in the quartz phenocrysts shows that some trace elements, including U, were affected by the post-magmatic processes. Their flat REE patterns accompanied by distinct negative Eu anomalies are typical of highly evolved F-rich leucogranites and rhyolites. Nd isotopic ratios ($\epsilon_{Nd(360)} = +0.6$ to -1.0) are similar to those of the felsic rocks of the Mount Pleasant complex. The Harvey rhyolites were generated by extensive fractional crystallization of andesites of the Mount Pleasant caldera. The melt evolved at the apex of the

magma chamber where volatile elements become concentrated. The Harvey rhyolite (with melt inclusions containing ~20 ppm U) had the potential to develop a significant U mineralization. The erupted glassy rhyolite is a favorable U source rock amenable to leaching by post-magmatic hydrothermal and meteoric water. The high Th/U ratios in the Harvey volcanic rocks compared to the low ratios in the U-rich melt inclusions is indicative of such a process.

Keywords Late Paleozoic · Rhyolite · Uranium · Mineralization · Fractional crystallization · Fluids

Introduction

Highly fractionated silica-rich felsic igneous rocks have attracted a large amount of attention in geological literature. One of the reasons for this interest is their distinct enrichment in rare metals, including radioactive elements—Th and U (e.g., Castor and Henry 2000; Cerny et al. 2005; Cuney and Kyser 2015; Nash 2010). Unlike the granitic rocks, there is only a rather limited amount of information on their volcanic equivalents even though felsic volcanic rocks have long been considered a primary source of uranium for many types of uranium deposits (e.g., Cuney and Kyser 2015; Nash 2010; Christiansen et al. 2015). In fact, there is still debate about the origin of these silica-rich rhyolites, particularly as the rocks commonly underwent late-magmatic or post-magmatic modification (e.g., Cuney and Kyser 2015; Hildreth and Wilson 2007; Nash 2010). There are two broad categories of petrogenetic models to explain the origin of silica-rich felsic magmas. The first category invokes a derivation from basaltic parent magma by fractional crystallization or by a combined process of fractional crystallization and assimilation. The second model assumes

Communicated by Timothy L. Grove.

Electronic supplementary material The online version of this article (doi:10.1007/s00410-016-1270-8) contains supplementary material, which is available to authorized users.

✉ J. Dostal
jdostal@smu.ca

¹ Department of Geology, Saint Mary's University, Halifax, NS B3H 3C3, Canada

² Shell Exploration, Houston, TX 77079, USA

³ Department of Earth Sciences, National Taiwan Normal University, 88 Tingzhou Road Section 4, Taipei 11677, Taiwan

basaltic magmas provided heat for the partial melting of crustal rocks (e.g., Clarke 1992; Winter 2001). The two processes have also been invoked for the origin of felsic magmas hosting U deposits (e.g., Cuney and Kyser 2015; Nash 2010), which are economically important and include the Streltsovskoye deposit (Transbaikalia, Russia) containing over 280,000 t of U_3O_8 (IAEA 2009; Cuney and Kyser 2015). The mechanisms facilitating U and Th enrichment in these rocks are poorly understood but can include both primary and secondary processes. In primary magmatic systems, these elements are typically incompatible and tend to become concentrated within highly evolved silica-rich melts, particularly during the latest stages of crystallization. Secondary uranium enrichment processes may involve an interaction of rocks with exsolved magmatic fluids or circulating heated meteoric water (e.g., Cuney and Kyser 2015; Nash 2010). In volcanic rocks, uranium mineralization is commonly concentrated in fracture-fill veins along which hot, metal-charged hydrothermal fluids have migrated.

To contribute to the debate on the origin and evolution of the rhyolitic rocks as well as to U mineralization, we investigated the Late Devonian–Early Carboniferous rhyolitic rocks of the Harvey Group in southwestern New Brunswick (Fig. 1) which hosts uranium mineralization (e.g., Gray et al. 2011; Hassan and Hale 1988; McLeod and Smith 2010; Payette and Martin 1986a, b). The purpose of the paper is to present the geochemical, isotopic and geochronological data on the volcanic rocks in order to constrain their origin, evolution and mineralization.

Geological setting

The Late Devonian to Early Carboniferous Harvey Group is a cover sequence of the Ganderia (Gander) terrane, one of the peri-Gondwanan terranes of the Northern Appalachians. The oldest known rocks in Ganderia are the Neoproterozoic arc-related volcanic and plutonic rocks which are overlain by Cambrian arc-back-arc sequences. Ensialic arc magmatism in Ganderia continued intermittently between 640 and 455 Ma (van Staal et al. 2012). In a southwestern part of the New Brunswick, these units are covered by Silurian metasedimentary rocks. The younger magmatic activities in the New Brunswick are Upper Silurian–Lower Devonian bimodal volcanic suites and granitoid plutons. The mafic volcanic rocks have within-plate characteristics (Dostal et al. 1989). The Late Devonian to Early Carboniferous period is marked by widespread bi-modal magmatic activities, particularly around the margin of the Maritimes Basin of the Northern Appalachians. The basin is a major Late Paleozoic successor basin (Gibling et al. 2009) that was initiated after the Early to Middle Devonian Acadian Orogeny (~400 Ma).

Felsic volcanic and volcanoclastic rocks of the Harvey Group occur along and form the base of the northern margin of the Fredericton sub-basin, the southwestern portion of the Maritimes Basin, in southwestern New Brunswick (Fig. 1a), approximately 40 km southwest of Fredericton (Fig. 1b). They form a NE-trending lens-shaped body about 15 km long and 3 km wide (Fig. 1b, c). This subaerial volcanic sequence overlies Silurian metasedimentary rocks, which outcrop to the northwest and in turn is overlain by clastic sediments of the Lower Carboniferous Shin (Bonaventure) and Upper Carboniferous Cumberland groups of the Maritimes Basin (Gibling et al. 2009), which are exposed to the southeast. The Harvey Group has been correlated with the rocks of the Piskahegan Group of the Mount Pleasant caldera complex, located on the southern limb of the sub-basin (Fig. 1b). Aeromagnetic and gravity surveys also suggest that the Harvey Group represents the northwestern margin of the Mount Pleasant complex (McLeod and Smith 2010), the site of a significant polymetallic (tin, tungsten, molybdenum, zinc, indium and bismuth) deposit (e.g., Sinclair et al. 2006; Thorne et al. 2013). Both the Harvey and Piskahegan groups are considered to be the remnants of an epicontinental caldera complex that formed during the initial stages of the development of the Maritimes Basin (McCutcheon et al. 1997; McLeod and Smith 2010).

The Late Paleozoic Maritimes Basin of the northern Appalachians covers the southern part of the Gulf of Saint Lawrence, Prince Edward Island and adjacent regions of New Brunswick and Nova Scotia (Fig. 1a). The basin contains several kilometers of middle Devonian to lower Permian strata. During the Late Devonian–Early Carboniferous the basin underwent an extension accompanied by pulses of igneous activities (Dunning et al. 2002). The Harvey as well as Piskahegan groups were emplaced during one of these pulses.

The Harvey Group (Fig. 1b, c) has been subdivided into three formations, from the bottom up: York Mills, Cherry Hill and Harvey Mountain (Beaudin et al. 1980; Payette and Martin 1986a, b). The York Mills Formation (~60 m thick) contains mostly sedimentary rocks including red sandstones, conglomerates and shale. There is, however, a volcanogenic component to the York Mills Formation, consisting of lithic and lapilli tuffs and laminated rhyolite flows and ignimbrites. The Cherry Hill Formation (~100 m thick) contains most of the U mineralization and is comprised of quartz–feldspar–phyric densely welded ash-flow tuff (“quartz–feldspar porphyry”), with poorly welded ash-flow sheets (Fig. 2) at the base and other ignimbrites and volcanoclastic sedimentary rocks. The Harvey Mountain Formation is a 75–100 m thick sequence composed of pyroclastic breccia, laminated rhyolite lava flows and ignimbrites intercalated with ash-fall tuffs.

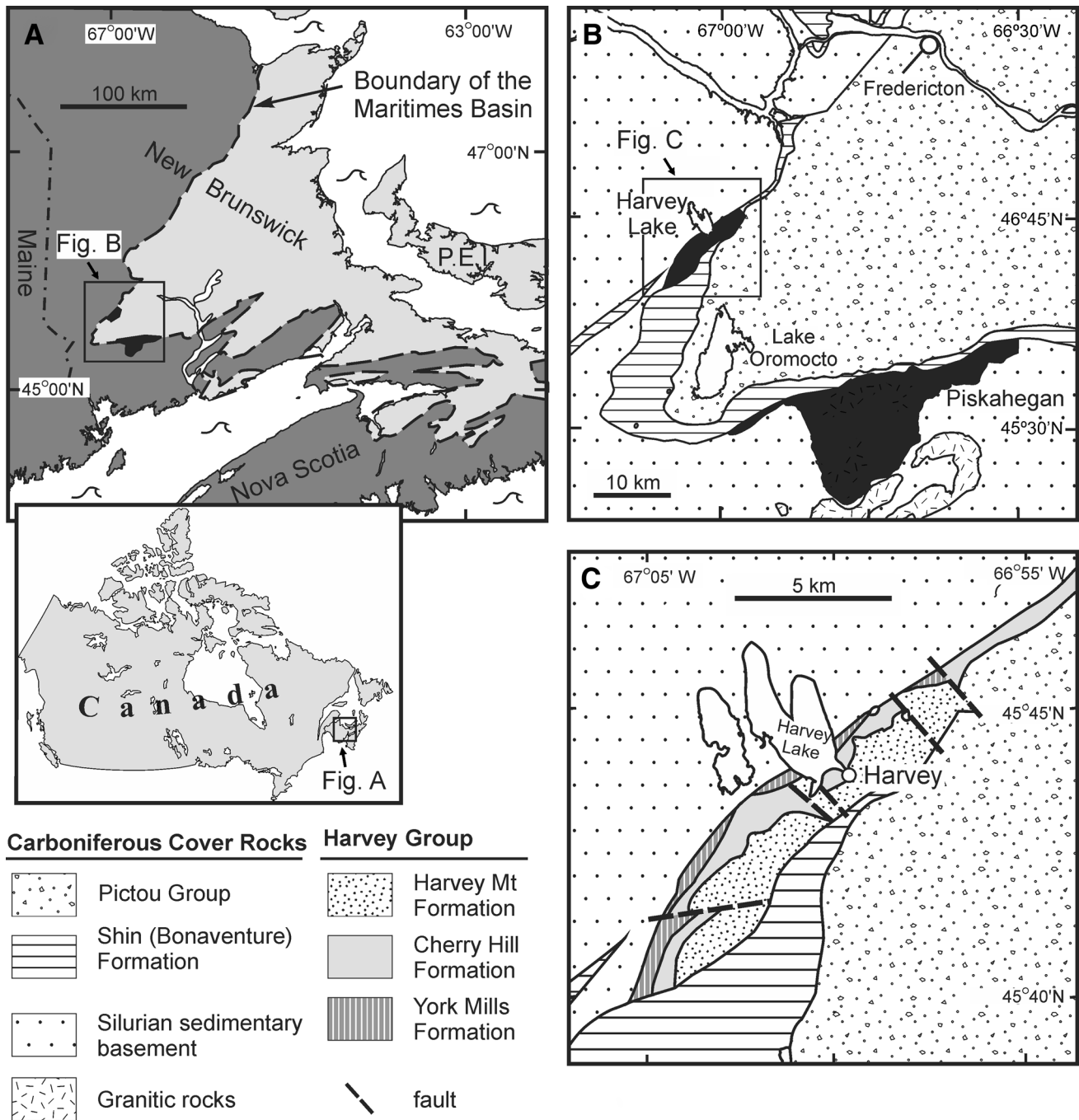


Fig. 1 a The map of a part of Atlantic Canada showing the boundary of the Maritimes Basin and the location of the Harvey and Piskahegan groups (black fields) as well as b. b Simplified geological map of the southwestern part of the Fredericton sub-basin and its envi-

rons showing the location of c. Black fields—volcanic rocks of the Harvey and Piskahegan groups. c Geological sketch map of the Harvey Group and surrounding area (modified after Payette and Martin 1986b). The insert (map of Canada) shows the location of a

Uranium mineralization

The Harvey Group has been the focus of uranium exploration for decades (e.g., Beaudin et al. 1980; Hassan and Hale 1988; McLeod and Smith 2010 and references therein). It contains several uranium prospects, but there has been no

production. Uranium mineralization of the Harvey Group has been classified as a volcanic- and/or caldera-related type (McLeod and Johnson 2007; McLeod and Smith 2010) and is confined to felsic volcanic and intercalated volcanoclastic and clastic sedimentary rocks. The mineralization appears to be stratabound and/or structurally

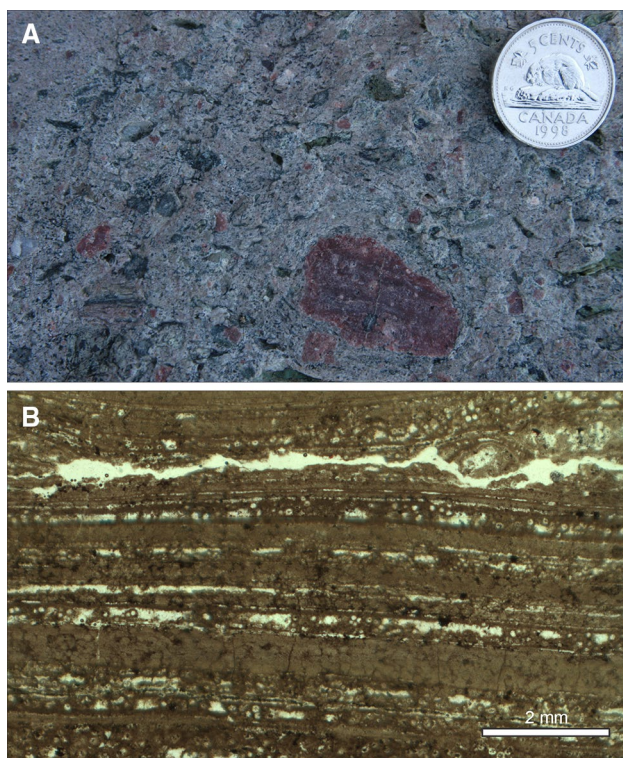


Fig. 2 **a** Weakly welded volcaniclastic rock of the Harvey Group (Cherry Hill Formation) containing lithic and mineral fragments enclosed in a fine-grained matrix composed mostly of broken shards, devitrified glass and microphenocrysts of quartz and feldspars. **b** Ignimbrite with laminated (flow-banding) texture defined by alternating aphanitic bands with layers containing microphenocrysts of quartz and feldspars or spherulites (Harvey Mountain Formation; plane-polarized light)

controlled and commonly associated with fluorite. The vein-type mineralization occurs in fracture zones and along permeable horizons within the volcanic piles (McLeod and Smith 2010). The fracture zones contain veins or lenses with pitchblende, pyrite, fluorite and secondary uranium minerals. Mineralization is also associated with chlorite-haematite and clay alteration zones and/or shear zones. Recent exploration reported values up to ~ 0.45 wt% U_3O_8 in welded ash-flow tuffs (ignimbrites) and volcaniclastic sediments (Cappella Resources Ltd. 2007).

Petrography

Field occurrences and petrography of the Harvey Group volcanic and volcaniclastic rocks were described by Beaudin et al. (1980), Gray (2010) and Payette and Martin (1986a, b). In general, the volcanic rocks of the Harvey Group are composed of quartz, plagioclase and K-feldspar set in a matrix of glass shards and very fine-grained material. Some rocks are porphyritic; the phenocrysts constitute

typically 10–15 vol% of the rocks. Plagioclase is more abundant than K-feldspar; both feldspars are not primary but re-equilibrated at low temperature after forming as phenocrysts. The plagioclase is typically albite and K-feldspar contains <5 % Ab component. Phenocrysts of biotite are rare and typically altered; silicification is widespread.

The Harvey Mountain Formation is composed primarily of rhyolitic ignimbrite with prominent laminated (flow-banding) texture (Fig. 2b) defined by alternating aphanitic bands 0.5–1 mm thick with 1–10 mm thick layers composed of microphenocrysts of quartz and feldspars (<1 mm in size) or greenish gray spherulites (up to 4 mm in diameter). The dominant aphanitic bands are devitrified and can contain numerous cavities filled by quartz and frequently coated by fluorite. The lamination of aphanitic rocks is also defined by iron coating. In the Cherry Hill Formation, quartz-feldspar porphyry (densely welded ash-flow tuff) is composed of phenocrysts of euhedral quartz and both feldspars (up to 5 mm in size). The phenocrysts constitute about 15–25 % of the rock and are enclosed in a matrix of devitrified welded shards. The matrix is typically purple and aphanitic. The Cherry Hill Formation is also made up of weakly welded volcaniclastic rocks which contain lithic and mineral fragments enclosed in a fine-grained matrix (Fig. 2a) composed mostly of broken shards, devitrified glass and microphenocrysts of quartz and feldspars. These rocks show a eutaxitic texture, defined by flattened devitrified shards and pumice fragments. The York Mills Formation includes slightly welded to non-welded pyroclastic flows and laminated rhyolites. Rhyolites with devitrified matrix contain small cavities lined with quartz, feldspars, opal and fluorite. Common accessory minerals in most rocks are zircon and apatite.

Payette and Martin (1986b) inferred that although the original texture is mostly preserved, the rocks were modified by high-temperature Na-metasomatism leading to pervasive albitization followed by low-temperature K-metasomatism, accompanied by silicification. During the silicification, albite was destroyed and Na removed from the rocks as K-feldspar grew. The rocks are generally devoid of fresh primary rock-forming minerals except quartz phenocrysts.

Analytical methods

Whole-rock major elements (Table 1, ESM for Appendix 1) were analyzed by X-ray fluorescence at the Department of Earth and Environmental Sciences of University of Ottawa, Ontario (Canada) using a Philips PW2400 spectrometer. Trace elements were determined using lithium metaborate–tetraborate fusion at the Activation Laboratories Ltd. in Ancaster, Ontario, by an inductively coupled plasma

Table 1 Major and trace element analyses of the rocks of the Harvey Group

Sample #	Cherry Hill Formation							
	NB-2	NB-5	NB-6	NB-11	NB-15	NB-16	NB-17	NB-20
SiO ₂ (wt%)	76.11	75.71	76.03	74.32	76.46	77.12	76.67	80.11
TiO ₂	0.07	0.08	0.08	0.58	0.11	0.08	0.09	0.09
Al ₂ O ₃	12.45	11.96	12.02	11.46	11.98	12.13	10.74	10.23
FeO*	1.29	1.54	1.40	1.93	1.78	1.36	1.20	1.24
MnO	0.02	0.02	0.02	0.11	0.01	0.01	0.01	0.01
MgO	0.09	0.08	0.08	0.99	0.20	0.18	0.25	0.24
CaO	0.45	0.83	0.58	1.67	0.32	0.26	0.08	0.08
Na ₂ O	3.53	3.53	3.49	2.98	2.32	3.12	1.28	1.18
K ₂ O	4.62	4.69	4.93	2.13	4.91	4.28	5.56	5.06
P ₂ O ₅	0.02	0.01	0.01	0.11	0.02	0.01	0.01	0.02
LOI	0.80	1.10	0.70	3.70	1.20	1.30	1.20	1.70
Total	99.45	99.55	99.33	99.98	99.32	99.85	97.10	99.96
V (ppm)	11	16	12	62	9	10	8	
Pb	33	67	45	17	34	49	63	54
Zn	110	110	96	114	108	104	95	106
Sn	18	15	12	5	19	23	15	14
W	3.3	6.2	5.7	6.60	8.2	4.3	4.8	6.8
Rb	463	473	481	174	491	471	508	453
Cs	9.8	10.3	8.7	8.6	13.2	11.1	25.4	15.0
Ba	36	29	26	198	67	10	13	13
Sr	31	39	34	118	30	60	38	34
Ga	29	29	25	14	29	30	24	23
Ta	6.61	6.1	6.59	2.21	6.2	6.0	4.3	4.2
Nb	59.7	81.3	65.4	39.0	62.7	71.5	46.9	47.6
Hf	8.1	8.9	8.4	8.3	8.4	8.7	6.8	6.3
Zr	148	164	161	294	158	161	140	146
Y	148	177	164	38	183	60.2	94	103
Th	37.0	38.1	41.7	15.7	38.6	26.6	27.3	26.1
U	3.32	4.0	4.0	13.3	4.6	4.2	4.40	5.1
La	28.4	28.2	29.4	32.9	76.3	2.3	9.10	8.3
Ce	67.1	78.5	67.5	80.0	156	6.2	22.5	27.7
Pr	10.1	11.5	10.6	7.56	24.1	0.82	2.72	3.0
Nd	50.2	47.3	55.3	29.0	122	4.0	12.3	15.0
Sm	15.8	17.9	17.5	6.93	37.5	1.53	3.68	5.75
Eu	0.06	0.05	0.07	0.93	0.32	0.01	0.03	0.04
Gd	17.4	22.7	19.2	6.12	39.5	2.68	8.91	11.6
Tb	3.74	4.64	4.09	1.09	6.52	0.82	2.20	2.68
Dy	25.3	31.7	28.0	6.79	37.0	7.29	15.9	18.0
Ho	5.23	6.23	5.74	1.37	6.97	2.02	3.46	3.9
Er	15.4	17.1	16.9	4.09	18.9	8.2	10.9	11.7
Tm	2.28	2.5	2.48	0.62	2.59	1.51	1.65	1.66
Yb	14.3	16.2	15.6	3.95	15.5	11.5	10.3	11.4
Lu	1.97	2.23	2.14	0.58	2.08	1.77	1.48	1.53

Table 1 continued

Sample #	Harvey Mt. Formation					York Mills Formation				
	NB-21	NB-22	NB-23	NB-25	NB-31	NB-26	NB-27	NB-28	NB-29	NB-30
SiO ₂ (wt%)	78.81	76.75	75.81	84.94	80.32	78.44	85.81	79.61	82.54	79.55
TiO ₂	0.07	0.08	0.07	0.05	0.06	0.06	0.05	0.06	0.06	0.08
Al ₂ O ₃	11.22	12.12	12.60	8.26	10.00	10.98	7.17	10.83	8.91	11.06
FeO*	0.28	1.16	1.09	0.30	0.52	0.95	0.78	0.76	0.95	1.06
MnO	0.01	0.02	0.02	0.01	0.01	0.01	0.02	0.02	0.01	0.01
MgO	0.11	0.44	0.48	0.16	0.23	0.24	0.16	0.21	0.19	0.17
CaO	0.08	0.18	0.18	0.10	0.05	0.12	0.13	0.08	0.09	0.47
Na ₂ O	1.53	1.78	1.70	2.16	0.20	1.53	0.83	1.54	1.27	5.56
K ₂ O	6.49	5.80	6.19	3.14	7.64	5.92	3.88	5.17	4.70	0.71
P ₂ O ₅	0.07	0.01	0.01	0.01	0.02	0.01	0.02	0.01	0.01	0.02
LOI	0.90	1.70	1.50	0.80	1.00	1.20	1.10	1.40	1.10	0.60
Total	99.57	100.03	99.65	99.93	100.07	99.48	99.94	99.69	99.83	99.3
V (ppm)	9	7	6		9	14	11	11	6	18
Pb	36	61	38	9	24	28	29	18	24	30
Zn	19	54	59	28	29	63	44	121	36	24
Sn	13	12	13	4	10	17	11	14	17	17
W	1.5	9.8	5.7	1.7	3.20	5.1	5.0	5.0	4.6	4.0
Rb	459	644	655	301	685	529	327	448	415	54
Cs	8.4	20.1	21.7	7.3	14.0	13.1	15.6	74.0	10.6	3.6
Ba	162	24	63	27	40	86	63	93	61	226
Sr	490	63	63	49	27	128	103	131	102	559
Ga	10	25	26	9	14	23	14	22	18	12
Ta	3.85	4.70	5.53	3.12	3.60	4.5	3.2	4.72	3.7	3.6
Nb	25.9	46.2	43.0	26.2	32.7	43.6	29.8	36.0	37.0	33.0
Hf	5.6	7.3	6.9	4.5	5.3	5.7	4.2	6.5	5.1	6.0
Zr	117	129	133	88	99	115	74	130	94	131
Y	81	94	96	47	40	102	42	82	69	94
Th	38.3	46.9	52.5	32.5	37.6	42.2	32.0	35.6	35.4	40.3
U	5.23	5.2	5.37	3.24	5.60	7.4	6.6	8.23	7.7	9.8
La	40.3	15.0	17.5	6.06	12.0	5.2	13.1	11.6	8.6	39.5
Ce	58.6	40.5	37.4	18.1	30.1	24.6	29.5	30.7	26.7	99.7
Pr	9.65	4.76	5.13	2.36	3.36	3.15	4.67	3.54	3.01	11.3
Nd	39.8	20.6	25.2	13.2	13.2	16.7	18.3	18.8	12.3	41.3
Sm	10.4	6.87	7.58	4.63	4.07	8.43	5.42	6.26	4.77	11.6
Eu	0.07	0.05	0.05	0.03	0.02	0.03	0.03	0.07	0.02	0.13
Gd	11.2	8.8	9.0	5.47	4.47	11.7	5.89	7.59	6.52	12.9
Tb	2.18	2.08	2.2	1.4	1.07	2.62	1.15	1.85	1.6	2.53
Dy	14.6	15.2	16.1	9.93	7.47	18.6	6.97	13.8	11.3	16.1
Ho	3.02	3.24	3.61	2.16	1.45	3.87	1.29	3.15	2.37	3.22
Er	9.34	10.6	11.0	6.57	4.78	11.9	3.97	9.96	7.64	9.99
Tm	1.36	1.63	1.66	0.97	0.76	1.79	0.61	1.56	1.19	1.37
Yb	8.19	10.8	10.9	6.07	5.03	11.8	4.29	10.7	7.92	9.34
Lu	1.16	1.55	1.55	0.82	0.75	1.59	0.62	1.6	1.13	1.24

FeO* total Fe as FeO, LOI loss on ignition

Table 2 Sm–Nd isotopic data for the rhyolitic rocks of the Harvey Group

Sample	Nd (ppm)	Sm (ppm)	$^{147}\text{Sm}/^{144}\text{Nd}$	$^{143}\text{Nd}/^{144}\text{Nd}_m$	2σ	$^{143}\text{Nd}/^{144}\text{Nd}_i$	$\varepsilon_{\text{Nd}(t)}$	T_{DM1} (Ma)	T_{DM2} (Ma)
<i>Cherry Hill Formation</i>									
NB-2	39.8	14.4	0.2185	0.512722	4	0.512207	0.64		
NB-11	28.0	6.44	0.1380	0.512266	4	0.511941	−4.56	1774	1559
NB-15	97.7	34.0	0.2103	0.512689	6	0.512193	0.37		
<i>Harvey Mountain Formation</i>									
NB-21	34.2	9.62	0.1701	0.512575	4	0.512174	−0.01	1996	1627
NB-23	19.5	6.85	0.2122	0.512643	7	0.512143	−0.06		
<i>York Mills Formation</i>									
NB-28	14.0	5.65	0.2440	0.512697	7	0.512122	−1.02		
NB-30	37.0	10.3	0.1683	0.512547	7	0.512150	−0.47	2010	1653

T_{DM1} depleted mantle model age calculated using a linear evolution for a mantle separated from the CHUR at 4.55 Ga and having a present-day ε_{Nd} value of +10, T_{DM2} depleted mantle model age calculated using the model of DePaolo (1988); $\varepsilon_{\text{Nd}(t)}$ values were calculated for the crystallization age $t = 360$ Ma, $^{143}\text{Nd}/^{144}\text{Nd}_m$ measured values, $^{143}\text{Nd}/^{144}\text{Nd}_i$ initial, calculated, 2σ uncertainty in measured $^{143}\text{Nd}/^{144}\text{Nd}$ —the value is the sixth decimal place

mass spectrometer (ICP–MS). Based on replicate analyses, the precision is generally between 2 and 10 % for trace elements and 2 % for major elements. The detection limits and information on the trace element analyses are available at the Activation Laboratories web site (www.actlabs.com).

Nd-isotope ratios of the rhyolitic rocks (Table 2) were determined at the Atlantic Universities Regional Facility at the Department of Earth Sciences of Memorial University of Newfoundland (St. John's, Newfoundland, Canada). Concentration data are standard ICP–MS analyses and are precise to ± 5 % (2σ). Ratios of $^{147}\text{Sm}/^{144}\text{Nd}$ were measured directly (without the separation) by ICP–MS with an estimated precision of ± 0.5 % (2σ). The isotopic ratios of $^{143}\text{Nd}/^{144}\text{Nd}$ were determined using a thermal ionization mass spectrometer operated in a static mode. Measured $^{143}\text{Nd}/^{144}\text{Nd}$ values were normalized to a $^{146}\text{Nd}/^{144}\text{Nd}$ ratio of 0.7219 calibrated to the JNdi-1 standard ($^{143}\text{Nd}/^{144}\text{Nd} = 0.512115$, Tanaka et al. 2000). An average value for $^{143}\text{Nd}/^{144}\text{Nd} = 0.511849$ resulted from replicate analyses of the LaJolla standard, which was determined repeatedly throughout the study. The 2σ values for all samples are less than or equal to 0.000008 for $^{143}\text{Nd}/^{144}\text{Nd}$ and are given in Table 2. $\varepsilon_{\text{Nd}(t)}$ values were calculated with respect to CHUR using a present-day $^{143}\text{Nd}/^{144}\text{Nd}$ ratio of 0.512638 and $^{147}\text{Sm}/^{144}\text{Nd}$ ratio of 0.196593 and subsequently age-corrected. T_{DM1} model age was calculated using a linear evolution for a mantle and having a present-day Epsilon value of +10. T_{DM2} model age was calculated according to the model of DePaolo (1988).

Zircons were separated from a quartz-feldspar porphyry sample from the Cherry Hill Formation (NB-17) for $^{206}\text{Pb}/^{238}\text{U}$ dating. The separated zircons were mounted in epoxy and photographed in backscattered and cathodoluminescence imagery. Zircon U–Pb isotopic analyses were performed by laser ablation ICP–MS at the National Taiwan University in Taipei, Taiwan. The full set-up and methods are described by Chiu et al.

(2009). The laser ablation (LA) was performed using a He gas carrier to improve material transport efficiency. Standard blanks were measured for ~ 1 min and calibration was performed using GJ-1 zircon standard, Harvard reference zircon 91,500 and Australian Mud Tank carbonatite zircon. Data processing was completed using GLITTER 4.0 software for the U–Th–Pb isotope ratios and common lead (Andersen 2002). Isoplot v. 3.0 was used to plot the Concordia diagram and to calculate the weighted mean U–Pb age (Ludwig 2001).

In situ zircon Hf isotope analyses (Table 3) of the sample NB-17 were carried out using a New Wave UP 213 LA microprobe, attached to a Nu Plasma multi-collector ICP–MS, coupled with a fixed detector array of 12 Faraday cups and 3 ion counters at the Institute of Earth Sciences, Academia Sinica in Taipei. Instrumental conditions, data acquisition, and analytical procedures were similar to Griffin et al. (2000, 2006). All results were calibrated to zircon standards, Mud Tank (Woodhead and Herget 2005) and 91,500 (Wiedenbeck et al. 1995), with typical within run precision (2σ) of ± 0.000030 on the $^{176}\text{Hf}/^{177}\text{Hf}$ analysis.

The $\varepsilon_{\text{Hf}(t)}$ values are calculated using chondritic ratios of $^{176}\text{Hf}/^{177}\text{Hf}$ (0.282785) and $^{176}\text{Lu}/^{177}\text{Hf}$ (0.0336) as derived by Bouvier et al. (2008). The ^{176}Lu decay constant of $1.865 \times 10^{-11} \text{ year}^{-1}$ reported by Scherer et al. (2001) is used in the calculation.

Geochronology

$^{206}\text{Pb}/^{238}\text{U}$ LA–ICP–MS geochronological dating of zircons from the Cherry Hill sample revealed a bimodal distribution of ages centered on a dominant 361 ± 7 Ma (MSWD = 1.7) and subordinate 403 ± 11 Ma (MSWD = 2.1; Fig. 3, Table 3; ESM for Appendix 2). The ~ 360 Ma age is interpreted as the age of the emplacement

of the Harvey Group volcanic rocks. These data are consistent with the age of the Piskahegan Group and the Mount Pleasant complex (e.g., Anderson 1992; McCutcheon et al. 1997; Thorne et al. 2013; Tucker et al. 1998) and the stratigraphic history of the basin. Older, early Devonian age (403 Ma) recorded by zircon likely represents the age of the contaminant of the parental magma (see below).

Geochemistry

Major elements

The Harvey Group volcanic rocks have variable major element compositions (Table 1) but compared to typical granites and rhyolites (e.g., Clarke 1992; Chayes 1985), they have high contents of SiO_2 (76–87 wt%; LOI-free) and alkalis with $\text{K}_2\text{O}/\text{Na}_2\text{O} > 1$ but are low in TiO_2 ($\sim < 0.1$ wt%), MgO (< 0.3 wt%), CaO (< 1 wt%) and P_2O_5 (< 0.03 wt%). On the quartz–alkali feldspar–plagioclase (QAP) diagram (Fig. 4), the Harvey rocks are scattered although most of them fall into the field of rhyolite, away from an average of the North American granitoid rocks (Chayes 1985). Their primary chemical compositions were modified by secondary processes as indicated by high values of SiO_2 (in some samples > 80 wt%), which are not representative of magmatic rocks. In order to evaluate the effects of various post-magmatic processes, Payette and Martin (1986a,b) and Gray et al. (2011) determined the compositions of the melt inclusions in quartz phenocrysts in these rocks (ESM for Appendix 3 and 4). A comparison of the whole-rock and the melt inclusion compositions shows some differences in the concentrations of the major elements. The melt inclusions have higher contents particularly of Al, Na and K than the whole rocks. On the QAP diagram (Fig. 4), whole rocks display a trend from the melt inclusions toward the Q apex. The whole rocks are higher in silica leading to a net dilution of other major elements. This is consistent with the observed silicification of the rocks, which was accompanied by K-metasomatism resulting in an increase of $\text{K}_2\text{O}/\text{Na}_2\text{O}$ but a drop of CaO and $\text{CaO}/\text{Al}_2\text{O}_3$ ratios at about 77 wt% SiO_2 (Fig. 5). The gradual decrease of Al_2O_3 , alkalis, FeO^* , and TiO_2 with increasing SiO_2 in the rhyolites is also consistent with fractionation of feldspars and minor amounts of biotite and Fe–Ti oxides although these trends, in part, also reflect silicification of the rocks. Low abundances of MgO , P_2O_5 and TiO_2 imply that both the rocks and melt inclusions are highly fractionated. The melt inclusions are peraluminous with aluminum saturation indices ($A/\text{CNK} = \text{molar } \text{Al}_2\text{O}_3/[\text{CaO} + \text{Na}_2\text{O} + \text{K}_2\text{O}] > 1$). Thus, it can be assumed that the peraluminous characteristics of the volcanic rocks represent the original magmatic features despite of their

alteration. Compositionally, both the rhyolites and melt inclusions share many similarities with evolved rhyolites and granites (including some felsic rocks from the Mount Pleasant complex) (e.g., Taylor 1992; Dostal and Chatterjee 1995; Linnen and Cuney 2005; Yang et al. 2003).

Payette and Martin (1986a,b) reported a F-bearing liquidus mineral (britholite) in the melt inclusions and inferred that the rhyolites are F-rich. Both Payette and Martin (1986 a,b) and Gray et al. (2011) reported the elevated F concentrations in the melt inclusions (> 0.2 wt%). In addition, fluorite, a secondary mineral, is abundant in the matrix and the vugs (e.g. Payette and Martin 1986a, b).

Trace elements

A comparison of chondrite-normalized rare earth element (REE) and primitive mantle-normalized trace element patterns of the whole rocks and glass of the melt inclusions (Figs. 6 and 7) shows that the abundances of high-field strength elements (HFSE), REE, Y and Th were not significantly affected by post-magmatic processes with the exception of a silica dilution effect. Relative to typical granitic and rhyolitic rocks (e.g., Clarke 1992; Cerny et al. 2005; Linnen and Cuney 2005), the rhyolites and melt inclusions are enriched in Rb, Th, U, Nb, Ta, Y and heavy REE (HREE).

According to immobile trace elements, the rocks are rhyolites (Fig. 8) and have within-plate characteristics (Fig. 9) in agreement with their emplacement during the early stages of basin extension. The abundances of several HFSE and REE such as Zr, Hf, Nb and Yb and the element ratios such as Yb/Nb (Fig. 10) in the rhyolites decrease with increasing SiO_2 , while the ratios of other elements such as including La/Yb (Fig. 10) do not change noticeably. The decrease of Yb/Nb ratio among others indicates that some of these trends are due to fractional crystallization. Compared to fractionated peralkaline granitic/rhyolitic rocks (e.g., Clarke 1992), they are enriched in Rb but depleted in Zr (Fig. 10). The rhyolites have also the low Zr/Y ratios (< 4). The distinct enrichment of Rb is also reflected in low K/Rb (80–110) and high Rb/Sr (~ 1 –30) ratios compared to typical upper crustal values (283 and 0.26, respectively, Rudnick and Gao 2003) but are similar to other anorogenic felsic rocks on the Rb/Sr versus K/Rb diagram (Fig. 11). The graph also shows that the distinct variations of the Harvey volcanics in the K–Rb–Sr space are mainly due to Sr, suggesting that Rb was probably not modified during the post-magmatic processes. Unlike the volcanic rocks, the melt inclusions are high in U (~ 20 ppm; Fig. 10).

The chondrite-normalized REE patterns of the rhyolitic rocks (Fig. 6) are relatively flat with $(\text{La}/\text{Yb})_n \sim 1$ (0.1–3) accompanied by distinct negative Eu anomalies ($\text{Eu}/\text{Eu}^* \sim 0.005$ –0.03). This type of pattern is rare among

Table 3 Results of zircon U/Pb geochronology and Lu–Hf isotopes for the Cherry Hill rhyolite

Spot	$^{206}\text{Pb}/^{238}\text{U}$	$\pm 1\sigma$	$^{207}\text{Pb}/^{235}\text{U}$	$\pm 1\sigma$	Error correc- tion	$^{206}\text{Pb}/^{238}\text{U}$ age (Ma ± 1 s)	$^{176}\text{Hf}/^{177}\text{Hf}$	$\pm 1\sigma$	$^{176}\text{Lu}/^{177}\text{Hf}$	$\pm 1\sigma$	$^{176}\text{Yb}/^{177}\text{Hf}$	$\pm 1\sigma$	I_{Hf}	$\epsilon_{\text{Hf}}(t)$	$\pm 1\sigma$
20	0.05917	0.00113	0.505	0.01346	0.7165	371 \pm 7	0.282824	0.00002	0.00146	0.00005	0.08476	0.0021	0.282814	9.7	0.8
17	0.06082	0.00144	0.51985	0.05432	0.2266	381 \pm 9	0.282829	0.00002	0.00158	0.00007	0.07463	0.00095	0.282818	9.9	0.7
5	0.05767	0.00124	0.43855	0.02857	0.3301	361 \pm 8	0.282665	0.00003	0.00384	0.00015	0.21257	0.0027	0.282639	3.5	1
22	0.05706	0.00113	0.49164	0.04105	0.2372	358 \pm 7	0.282641	0.00003	0.00323	0.00025	0.18784	0.016	0.282619	2.8	1.1
11	0.05699	0.00118	0.49296	0.02555	0.3995	357 \pm 7	0.282664	0.00002	0.0024	0.00007	0.12648	0.0016	0.282648	3.8	0.8
9	0.05772	0.00111	0.44835	0.01207	0.7143	362 \pm 7									
15	0.06107	0.00211	0.78914	0.15058	0.1811	382 \pm 13	0.282673	0.00003	0.0015	0.00004	0.00788	0.0011	0.282663	4.4	0.9
14	0.05601	0.0012	0.45602	0.03029	0.3226	351 \pm 7									
10	0.05557	0.00139	0.41752	0.05033	0.2075	349 \pm 8	0.282762	0.00002	0.00185	0.00012	0.08355	0.0023	0.282749	7.4	0.7
8	0.05667	0.0011	0.43493	0.01214	0.6954	355 \pm 7	0.282629	0.00003	0.00137	0.00003	0.00698	0.0013	0.28262	2.8	1
4	0.06695	0.00146	0.51389	0.03415	0.3282	418 \pm 9	0.282785	0.00003	0.00059	0.00067	0.02502	0.00067	0.282781	9.5	1
12	0.06746	0.00152	0.52206	0.04873	0.2414	421 \pm 9	0.282745	0.00002	0.00194	0.00014	0.10121	0.004	0.28273	7.7	0.7
13	0.06269	0.00207	0.7291	0.13919	0.173	392 \pm 13									
19	0.06275	0.00118	0.48783	0.01162	0.7895	392 \pm 7	0.282661	0.00003	0.00199	0.00005	0.08856	0.0011	0.282646	4.7	0.9
21	0.06247	0.00124	0.54002	0.0422	0.254	391 \pm 8	0.282744	0.00002	0.00123	0.00001	0.06907	0.004	0.282735	7.9	0.8
7	0.06463	0.00128	0.47371	0.01556	0.6029	404 \pm 8	0.282693	0.00003	0.00051	0.00003	0.02322	0.0014	0.282689	6.2	0.9
18	0.06531	0.00122	0.50696	0.01186	0.7985	408 \pm 7	0.282628	0.00003	0.00111	0.00002	0.06408	0.00078	0.282674	5.7	0.9

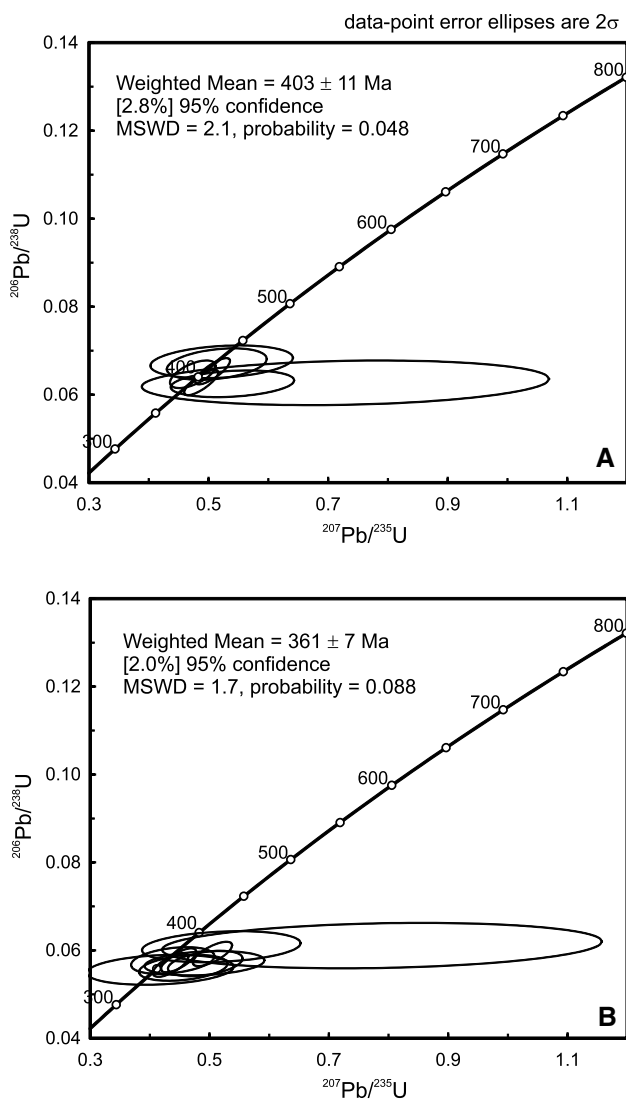


Fig. 3 Concordia plot for LA-ICP-MS zircon U–Pb dating results for rhyolite from Cherry Hill Formation of the Harvey Group. **a** Grouping of ~400 Ma zircons and **b** grouping of ~360 Ma zircons

felsic igneous rocks but is associated with highly fractionated F-rich leucogranites and rhyolites (Fig. 6) (e.g., Irber 1999; Christiansen et al. 1984, 1986; Dostal et al. 2004; Taylor 1992; Yang et al. 2003). Bau (1996) named such patterns as “tetrad REE patterns”. The mantle-normalized trace element plots of the Harvey rocks also show a significant depletion in Sr, Ba, Eu and Ti, which reflects the highly evolved nature of the rocks (Fig. 7). Other characteristics of the patterns are relative enrichments in Rb, Ta and Hf accompanied by a depletion of Nb relative to Ta and Zr relative to Hf. Relative to typical crustal value of ~37 (e.g., Rudnick and Gao 2003; Shaw et al. 1976), the rocks have low Zr/Hf (~20) ratio. In general, these patterns are similar to those of metal-rich leucogranites and rhyolites (e.g., Cerny et al. 2005; Linen and Cuney 2005; Dostal 2016 and references therein).

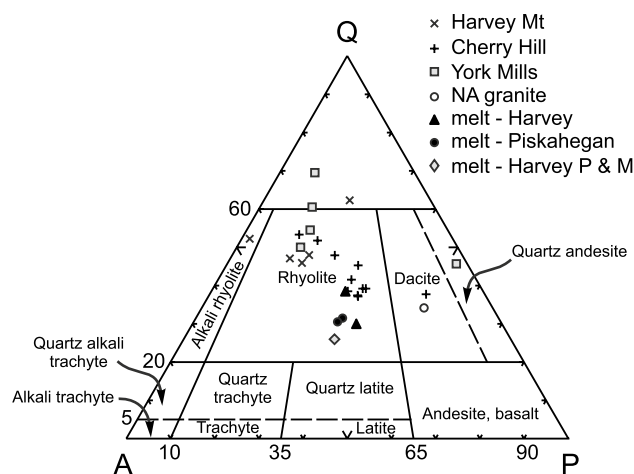


Fig. 4 Quartz–alkali feldspar–plagioclase (QAP) classification diagram used to characterize the modal composition of the volcanic rocks (modified after Le Maitre et al. 1989). The plot illustrates the composition of the Harvey Group felsic volcanic rocks. The compositions of the melt inclusions of the Harvey and Piskahegan groups (Gray et al. 2011; melt-Harvey and melt-Piskahegan) and the Harvey Group (Payette and Martin 1986a, 1986b; melt-Harvey P&M) as well as the average of the North American granitoid rocks (NA granite) of Chayes (1985) are shown for comparison

Isotopes

Nd isotopic ratios for the Harvey rocks are given in Table 2 where they are aged-corrected to 360 Ma. The $\epsilon_{\text{Nd}(t)}$ values (+0.6 to –1.0) for the Harvey rhyolitic rocks are similar to the values of felsic rocks of the Mount Pleasant caldera (Anderson 1992; McCutcheon et al. 1997) and Devonian–Carboniferous topaz-bearing granitic plutons of Whalen et al. (1996) from this part of the New Brunswick (Fig. 12). The ages and tectonic settings of the rocks of the Mount Pleasant complex are comparable to those of the Harvey Group. All of these rocks also plot within the range of Devonian–Carboniferous felsic rocks of the Maritimes Basin in New Brunswick and Nova Scotia (Keppie et al. 1997; Pe-Piper and Piper 1998). The $\epsilon_{\text{Hf}(t)}$ zircon values yielded an average value of 7.0 ± 1.7 (MSWD = 3.4) for the age of 403 Ma (range 4.7–9.5) and a value of 6.3 ± 2.6 (MSWD = 13) for the age of 360 Ma (2.8–9.9; Table 3). The values for 403 Ma are assumed to represent a mid-crustal contaminant of the Harvey magma.

Discussion

Petrogenesis

The volcanic rocks of the Harvey Group were emplaced contemporaneously with the formation of the Mount Pleasant caldera complex (~360–370 Ma; Anderson 1992;

Fig. 5 Variation diagrams of major elements and their ratios for the Harvey rhyolitic rocks using SiO₂ as a differentiation index. Melt inclusions from quartz phenocrysts of the Harvey and Piskahegan rhyolitic rocks (Gray et al. 2011: melt-Harvey; melt-Piskahegan and Payette and Martin 1986a, 1986b: melt—Harvey P&M) are also shown for comparison

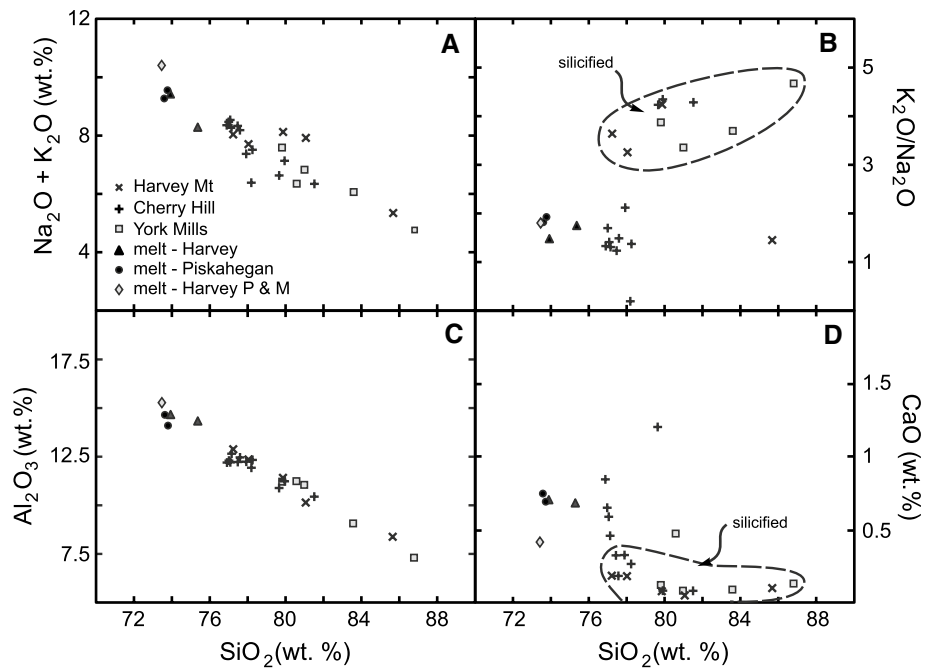


Fig. 6 Chondrite-normalized rare earth element patterns of the Harvey rhyolitic rocks. Melt inclusions from quartz phenocrysts of the Harvey (Cherry Hill Formation) and Piskahegan rhyolitic rocks (Gray et al. 2011) as well as the topaz-bearing rhyolite from the Spor Mountain, Utah (Christiansen et al. 1984), F-rich granites from Mount Pleasant granitic suite (Yang et al. 2003) and Li-F-rich leucogranite from the Davis Lake pluton, Nova Scotia (Dostal and Chatterjee 1995; Dostal et al. 2004) are also shown for comparison. Normalizing values are after Sun and McDonough (1989). **a** Harvey Mountain Formation; **b** Cherry Hill Formation; **c** York Mills Formation; **d** melt inclusions from Harvey rhyolites (Cherry Hill Formation); **e** melt inclusions from Piskahegan rhyolites; **f** Spor Mountain (sample SM-31); DLP-Davis Lake pluton (sample 79-100), MPG-Mount Pleasant granite (PRL-95-1-1771)

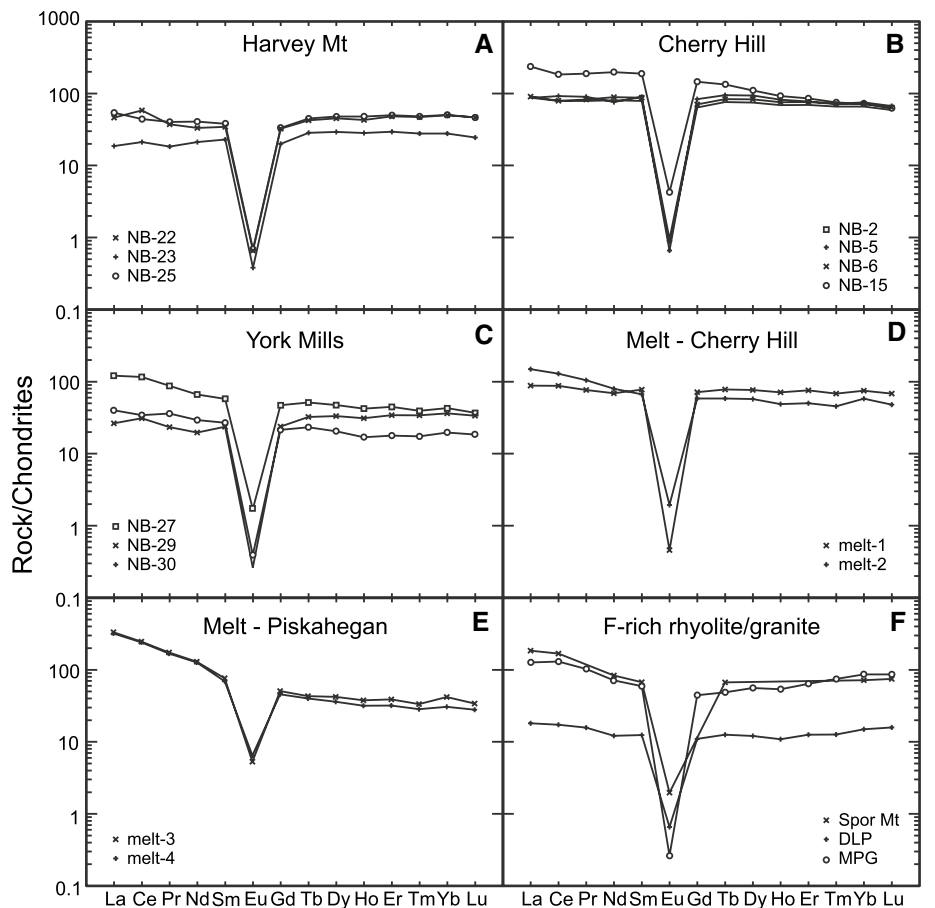


Fig. 7 Primitive mantle-normalized incompatible element patterns of the Harvey rhyolitic rocks. Melt inclusions from quartz phenocrysts of the Harvey (Cherry Hill Formation) rhyolitic rocks (Gray et al. 2011) are also shown for comparison. Normalizing values are after Sun and McDonough (1989). **a** Harvey Mountain Formation; **b** Cherry Hill Formation; **c** York Mills Formation; **d** melt inclusions of the Harvey rhyolites (Cherry Hill Formation)

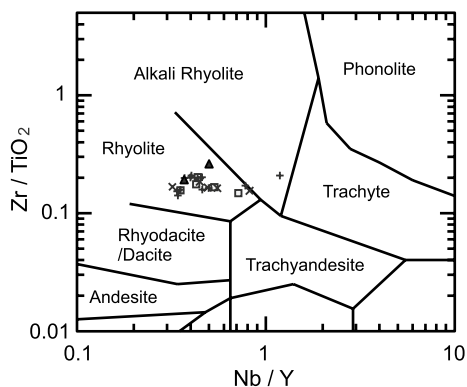
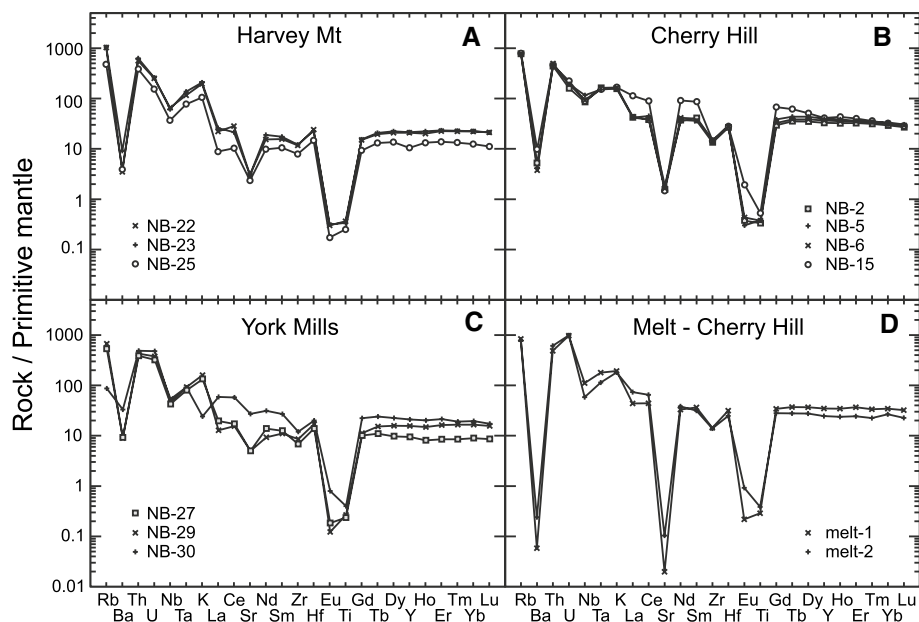


Fig. 8 Zr/TiO_2 versus Nb/Y classification diagram of Winchester and Floyd (1977) for rhyolitic rocks of the Harvey Group. Melt inclusions from quartz phenocrysts of the Harvey rhyolitic rocks (Gray et al. 2011) are also shown for comparison. Symbols Harvey Mountain Fm (cross); Cherry Hill Fm (plus); York Mills Fm (square box); melt inclusions of Harvey Group (triangle)

McCutcheon et al. 1997; Thorne et al. 2013, including emplacement of volcanic rocks of the Piskahegan Group dated at 363.8 ± 2.2 Ma; Tucker et al. 1998). This contemporaneity supports an inference of McLeod and Smith (2010), among others, that the Harvey Group is a north-western extension of the Mount Pleasant caldera (Fig. 1).

The Harvey volcanic rocks (and their melt inclusions) are peraluminous rhyolites that were emplaced in a within-plate environment (Fig. 9), which is consistent with their geological setting characterized by extension-related tectonics and rifting associated with the opening of the Maritimes Basin. The low contents of Ti, Mg and P in the volcanic rocks imply that they are highly evolved. Assuming that the melt inclusions represent the parent magma, the

variation trends of major and trace elements suggest that the Harvey volcanic rocks were produced by fractional crystallization of feldspars and minor amounts of biotite, Fe–Ti oxides and accessory minerals. However, the rocks underwent post-magmatic hydrothermal alterations which partially modified their compositions. The alteration included silicification and K-metasomatism accompanied by changes in K_2O/Na_2O and CaO/Al_2O_3 ratios at about 77 wt% SiO_2 (Fig. 5).

Several models have been invoked for the origin of within-plate rhyolitic rocks such as those of the melt inclusions. They include (1) partial melting of a crustal source (e.g., Sisson et al. 2005), (2) combined assimilation–fractional crystallization (AFC) of basaltic magmas (e.g., Marks and Markl 2001) and (3) extensive fractional crystallization of mafic or intermediate magma (e.g., Turner et al. 1992).

A number of partial melting, fractional crystallization and assimilation–fractional crystallization processes for the origin of the melt inclusions of the Harvey Group have been evaluated using geochemical model calculations. The most robust results were those obtained by fractional crystallization of the andesitic rocks of the Mount Pleasant caldera, in particular of South Oromocto andesites (Anderson 1992; McCutcheon et al. 1997). The andesites were interpreted to be the result of AFC processes involving the crustal contamination of rift-related tholeiitic basalts and of a change from non-oxic to oxidizing conditions accompanied by a relatively high content of magmatic water. As the andesitic rocks contain hornblende indicative of mid-crust crystallization and show a calc-alkaline fractionation trend that is typical of high $P_{(tot)}$ and P_{H_2O} conditions, the contamination had to take place at a deeper crustal level (e.g.,

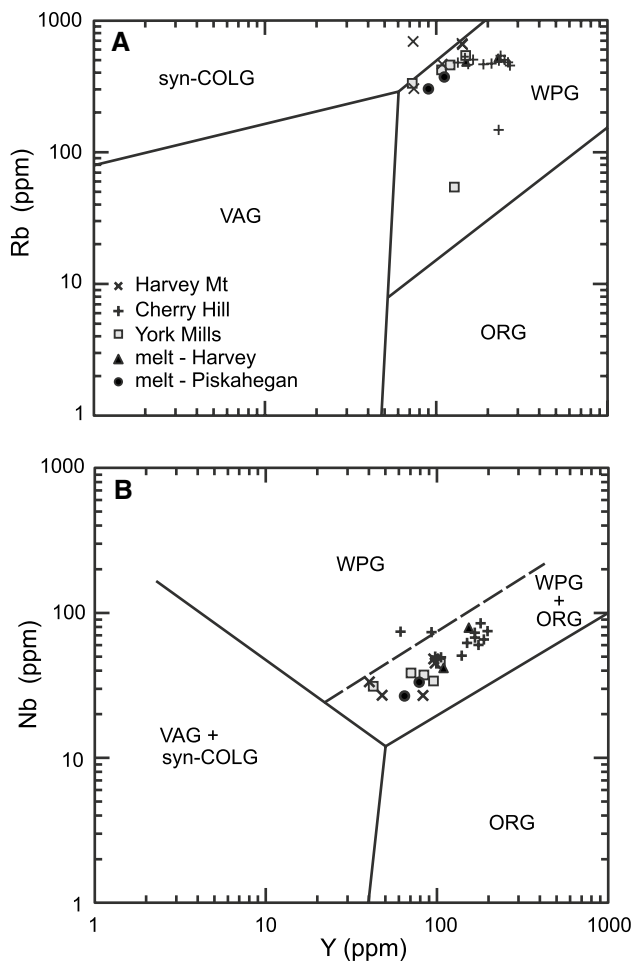


Fig. 9 a Rb versus (Nb + Y) and b Nb versus Y (in ppm) tectonomagmatic discrimination diagrams of Pearce et al. (1984) for rhyolitic rocks of the Harvey Group. Melt inclusions from quartz phenocrysts of the Harvey and Piskahegan rhyolitic rocks (Gray et al. 2011) are also shown for comparison. *Fields* ORG ocean ridge granites, VAG volcanic arc granites, *syn-COLG* syn-collisional granites, WPG within-plate granites

Osborn 1959; Zimmer et al. 2010). Although the contaminant was a middle crust source, such a rock was not a granulite. Granulites are typically depleted in U (Dostal and Capedri 1978). The contaminant was probably fluid-rich phlogopite/biotite-bearing mid-crustal metasedimentary rock. The 403 Ma inherited zircon age obtained from the Harvey rhyolite probably reflects the age of such a contaminant. The Piskahegan rhyolites are probably correlative of the Harvey rocks although they appear to be less evolved.

Model calculations

The petrological evolution of mafic liquids can be modeled using MELTS software (Ghiorso and Sack 1995; Smith and Asimow 2005). MELTS is calibrated for a wide range of silicate bulk compositions that encompass nearly the

entire spectrum of igneous rocks. The software permits the adjustment of magmatic conditions (i.e., relative oxidation state, pressure and water content) of the parental composition. The adjustment of the magmatic conditions allows the user to test a variety of hypotheses that are not necessary related to the parental composition but can provide better constraints on possible liquid evolution.

Fractional crystallization modeling was carried out using a starting composition of South Oromocto andesite from the Mount Pleasant caldera complex (Table 4) in attempt to replicate the petrogenesis of the Cherry Hill Formation and Piskahegan Group melt inclusions (ESM for Appendix 3). The relative oxidation state (i.e., $f_{O_2} = \text{FMQ } 0$) and initial water contents (i.e., 2 wt%) used in the model are typical of basaltic andesites, but there is limited geological evidence to constrain the pressure of fractionation; therefore, we attempted modeling at a variety of pressures (Moore and Carmichael 1998; Benjamin et al. 2007). Rare earth elements (i.e., La, Yb) were also included in the model to monitor their behavior during the liquid evolution, in particular to determine whether the flat chondrite-normalized patterns are related to magma evolution or to other processes.

The liquid evolution results (black circles), at 10 °C intervals, are shown in Fig. 13 and represent the starting composition under the magmatic conditions outlined in Table 4. The models were broadly able to produce compositions similar to the melt inclusions at a pressure of 0.6 GPa (i.e., 6 kbar). The modeled crystallization sequence is as follows: orthopyroxene (1170–1120 °C), diopside-augite (1110 °C), pigeonite (1110–860 °C), Ti-magnetite (1070–920 °C), plagioclase (1130–720 °C), apatite (1030–820 °C), ilmenite (920–720 °C), alkali feldspar (920–720 °C) and garnet (850–720 °C). The proportions of the minerals, compositions and their temperature range are shown in Table 5. Interestingly the model indicates that garnet will crystallize at 850 °C although garnet is not observed in magmatic rocks of the Mount Pleasant complex. Consequently we ran a “garnet-free” model with identical parameters as in Table 4 but suppressed garnet crystallization. The garnet-suppressed model is shown as the white circles (at 10 °C intervals) in Fig. 14, and the results are summarized in Table 6. The main difference between the two models is that pigeonite crystallizes to 720 °C, whereas in the garnet model it stops crystallizing at 860 °C. Although both models show very good agreement with nearly all major elements, CaO, P_2O_5 and K_2O are not well replicated.

The CaO and P_2O_5 may be due to lower amounts (i.e., <1 %) of apatite fractionation in the model. If the model is adjusted to incorporate more apatite (i.e., ~1 % to ~2 %) fractionation, then the CaO content drops closer (i.e., ~0.9 wt%) to the melt inclusion compositions

Fig. 10 Variation diagrams of trace elements and their ratios for the Harvey rhyolitic rocks using SiO_2 as a differentiation index. Melt inclusions from quartz phenocrysts of the Harvey and Piskahegan rhyolitic rocks (Gray et al. 2011: melt-Harvey; melt-Piskahegan) are also shown for comparison. Note that the melt inclusions of Harvey and Piskahegan groups have different concentrations of Zr, Yb and U as well as the different La/Yb ratios

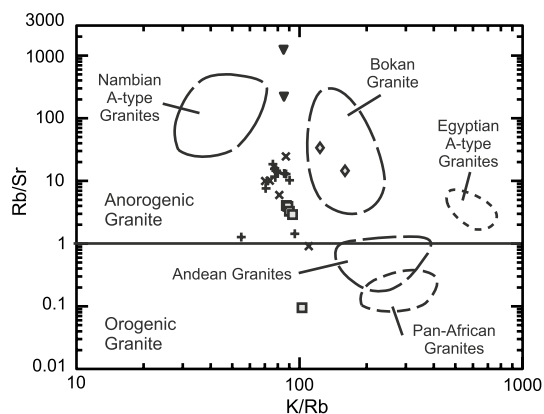
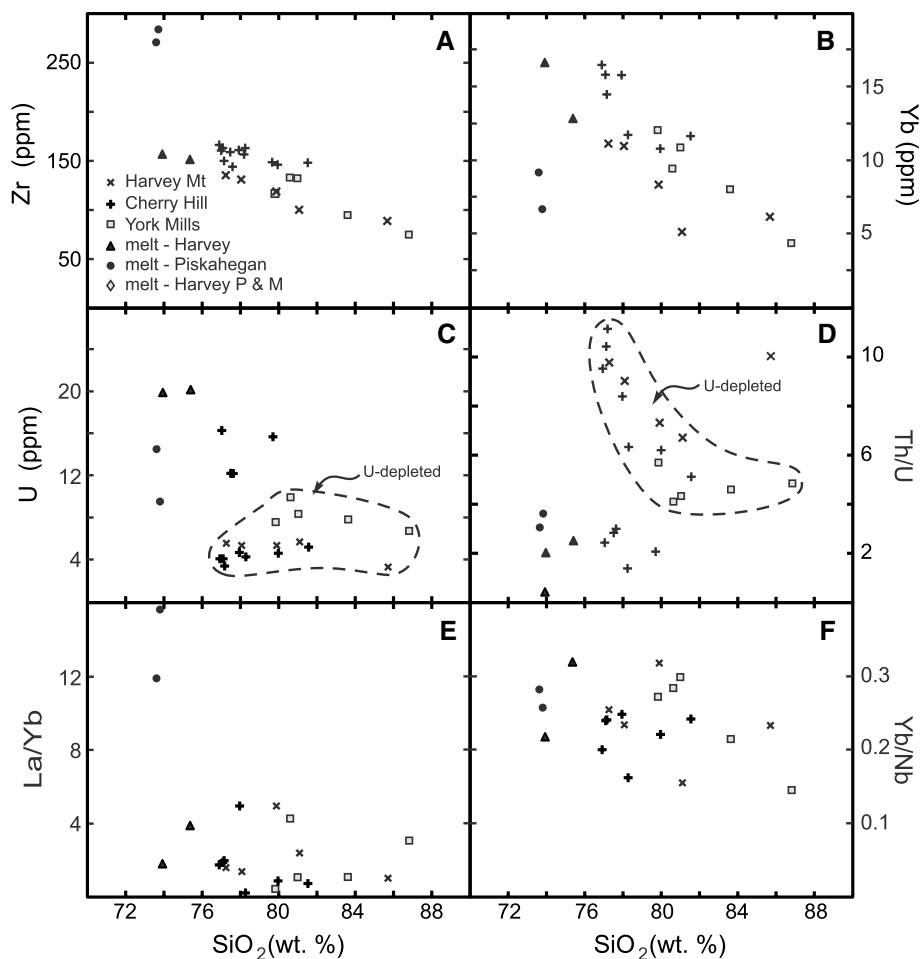


Fig. 11 Rb/Sr versus K/Rb plot for the Harvey rhyolitic rocks. The melt inclusions as well as most Harvey rocks have Rb/Sr ratios >1 . The boundary (at Rb/Sr = 1) that separates the fields of orogenic and anorogenic granites and rhyolites as well as the fields for various granitic rocks are after Abdel-Rahman (2006). The field for the Bokon (A-type) granite is after Dostal et al. (2014). The abundances of Sr are dominant variables. Symbols: Harvey Mountain Fm (cross); Cherry Hill Fm (plus); York Mills Fm (square box); melt inclusions of Harvey Group (triangle)

(i.e., ≤ 0.7 wt%) (Fig. 14). Additional apatite fractionation could explain the composition of the melt inclusions from the Piskahegan Group as they have much higher LREE concentration than the Cherry Hill melt inclusions (Fig. 6; ESM for Appendix 3). However, the melt inclusions from the Cherry Hill Formation have much lower La than the Piskahegan melt inclusions but have similar P_2O_5 content (i.e., <0.05 wt%). A possible explanation is that the Cherry Hill melt inclusions experienced monazite fractionation rather than apatite fractionation as the partition coefficients (K_d) of La in apatite (<25) and La in monazite (~ 100 or higher) are significantly different (Fujimaki 1986; Stepanov et al. 2012). Using the mineral proportions outlined (substituting monazite for apatite) in Table 6 and K_d values of La and Yb in clinopyroxene ($K_{d_{\text{La}}} = 0.014$; $K_{d_{\text{Yb}}} = 0.09$), plagioclase ($K_{d_{\text{La}}} = 0.013$; $K_{d_{\text{Yb}}} = 0.02$), alkali feldspar ($K_{d_{\text{La}}} = 0.08$; $K_{d_{\text{Yb}}} = 0.03$) and monazite ($K_{d_{\text{La}}} = 119$; $K_{d_{\text{Yb}}} = 13$) in basaltic andesite, we demonstrate in Fig. 13f that a possible monazite fractionation path could explain the depleted LREE patterns of the Cherry Hill inclusions. If monazite

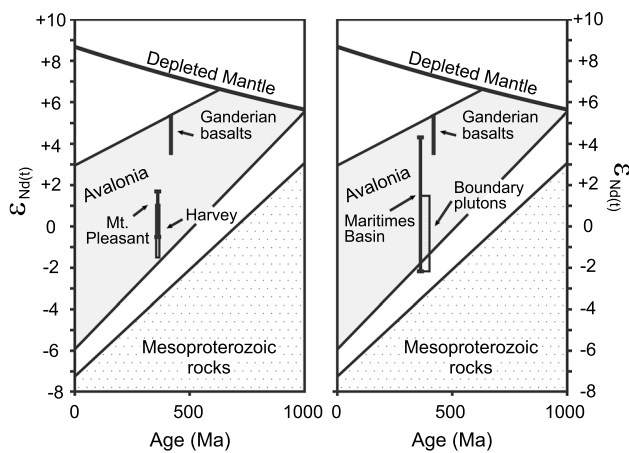


Fig. 12 $\epsilon_{Nd(t)}$ versus time plot comparing new Sm–Nd isotopic data of the Harvey Group rhyolites with a compilation of Sm–Nd isotopic data for the Siluro-Devonian basalts of the Gander terrane (Dostal et al. 2016), felsic rocks of the Mount Pleasant caldera (Anderson 1992), Devonian “boundary” (topaz-bearing) granitic plutons (Whalen et al. 1996) and Devonian–Carboniferous felsic rocks of the Maritimes Basin in Nova Scotia and New Brunswick (Keppie et al. 1997; Pe-Piper and Piper 1998). Shaded area is the Avalonian basement and subcontinental lithospheric mantle (after Keppie et al. 2012; Murphy et al. 2011). The field for Mesoproterozoic rocks is from Murphy et al. (2008)

Table 4 MELTS model composition and parameters

Sample	38-C (rock data)	38-C (model)
SiO ₂ (wt%)	55.15	55.98
TiO ₂	1.53	1.55
Al ₂ O ₃	15.85	16.09
FeO _t	7.67	7.79
MnO	0.14	0.14
MgO	3.43	3.48
CaO	5.78	5.87
Na ₂ O	3.48	3.53
K ₂ O	3.01	3.06
P ₂ O ₅	0.50	0.51
H ₂ O		2.0
La (ppm)	46.3	46.3
Yb	3.86	3.86
fO ₂		FMQ 0
Pressure (GPa)		0.6

Major element data for model normalized to 100 % including water. Rock data from Gray (2010)

is the principal phosphate mineral to fractionate to produce the Cherry Hill inclusion compositions, then an additional mineral must be responsible for the depletion of CaO. The most likely candidate to reduce CaO without affecting P₂O₅, other major elements or the HREE and Y is fluorite as it is known to be present within the Harvey volcanic rocks.

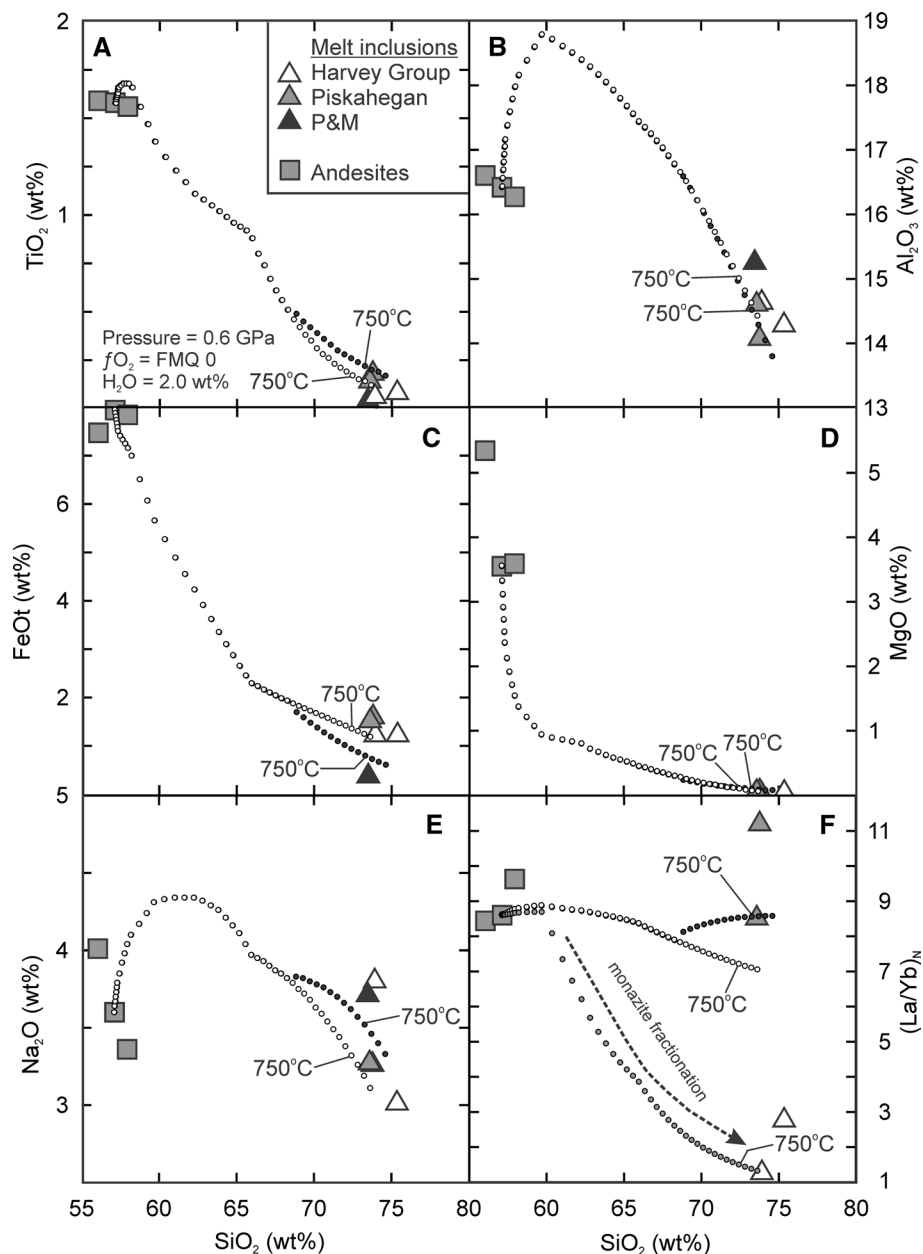
The discrepancy between the K₂O content is problematic as the melt inclusions have ~6 wt%, whereas the model predicts ~3.5 at ~75 wt% SiO₂. The reason for the difference between the modeled and measured K₂O is uncertain, but it could be due to subsequent assimilation of potassic siliceous fluids into the magma system during fractionation or limitations of the modeling software but most likely the major issue is the fact that the starting compositions of the model is restricted largely due to the limited published data on the South Oromocto andesites (Anderson 1992; McCutcheon et al. 1997; Gray 2010). Furthermore, the South Oromocto andesites have experienced post-emplacment alteration to varying degrees (Anderson 1992; McCutcheon et al. 1997). Although the models show general agreement between the liquid evolution curves and the bulk composition of the melt inclusions, there are a number of uncertainties (i.e., exact parental magma composition) that prevent a more definitive result. We cannot rule out the possible influence of F-rich fluids in the system and that the Cherry Hill Formation and Piskahegan Group melt inclusions, although from the same complex, represent different magma batches or experienced slight differences (e.g., crustal assimilation, influence of hydromagmatic fluids) in their petrogenesis that cannot readily be modeled.

Nd isotopes and REE distributions in the rhyolites

Similarities of $\epsilon_{Nd(t)}$ in the rhyolites suggest that the Nd isotopic system was not disturbed by hydrothermal fluids. The $\epsilon_{(t)}$ values of the Harvey rhyolitic rocks show a good agreement with the data of Anderson (1992) and McCutcheon et al. (1997) for the felsic rocks of the Mount Pleasant complex. An exception is one sample (NB-11), which has a high negative value (−4.6) probably reflecting upper crustal contamination as also suggested by chemical composition. The $\epsilon_{Nd(t)}$ values (~0) of both Harvey and the Mount Pleasant caldera negate a significant contribution from substantially older continental crust or sedimentary rocks derived from it. The rocks plot into the field of Avalonian and peri-Rodanian lithosphere (Fig. 12) and their $\epsilon_{Nd(t)}$ values are consistent with derivation from a subcontinental lithospheric mantle with a contribution from a middle crust. The slightly lower ϵ_{Hf} zircon values for the Harvey (360 Ma) magma than for the 403 Ma zircon indicate a possible addition of a contaminant with higher $\epsilon_{Hf(t)}$, but the analytical precision does not permit a conclusive answer.

The flat chondrite-normalized REE patterns with distinct negative Eu anomalies of the felsic rocks are relatively rare and controversial. They are mostly restricted to highly fractionated granites. These “tetrad-like” rare earth patterns have been attributed to fluid–rock or fluid–melt interactions during late-magmatic stages (e.g., Bau 1996, Irber 1999; Jahn et al. 2001; Monecke et al. 2002). Veksler et al. (2005)

Fig. 13 Major and trace elemental results of MELTS modeling showing the liquid evolution curves of the starting composition (Table 4). The *black circles* represent liquid compositions at 10 °C intervals. The *white circles* represent liquid compositions at 10 °C intervals in the garnet suppression model. The *gray circles* in *panel f* represent the liquid compositions in the monazite fractionation model. Additional data from Gray (2010)



inferred that these patterns are related to the partitioning of REE between silicate melts and coexisting fluoride melts. Alternatively, Yurimoto et al. (1990), Duc-Tin and Keppler (2015) and others argued that the shape is the result of crystallization and removal of accessory phosphate phases, most notably monazite and apatite.

The scanning electron microscope observation indicates that the bulk of REE occurs in accessory phases, like in many other felsic rocks. As the melt inclusions and whole rocks have rather similar REE patterns, the magma was modified by a fluid–melt interaction or by a separation of accessory minerals prior to incorporation into quartz crystals. The model calculations show that

crystallization of accessory phases from an andesitic parent can account for the flat REE patterns of the Harvey rocks. However, the presence of fluorite in the Harvey sequence and the elevated concentrations of F in the melt inclusions suggest that these highly fractionated melts formed at the top of felsic magma chamber where volatile elements (F, Cl, water) also become concentrated and could have interacted (e.g., Nash 2010) and produced the “tetrad” REE patterns (Veksler et al. 2005). It appears that either or both processes (fractional crystallization of accessory phosphates and fluid–melt interaction) could be involved in the generation of the “tetrad-like” rare earth patterns.

Table 5 Proportion and composition of crystallized minerals

Mineral	T (°C)	Composition	Amount crystallized (%)
Orthopyroxene	1170	Wo ₃ En ₇₄ Fs ₂₃	4.9
	1120	Wo ₄ En ₆₉ Fs ₂₇	
Clinopyroxene	1110	Wo ₃₈ En ₄₃ Fs ₁₉	0.3
Pigeonite	1110	Wo ₁₃ En ₅₇ Fs ₃₀	14.5
	860	Wo ₆ En ₄₄ Fs ₅₁	
Plagioclase	1030	An ₄₈ Ab ₄₈ Or ₄	32.6
	720	An ₂₁ Ab ₇₂ Or ₇	
Alkali feldspar	910	An ₄ Ab ₃₄ Or ₆₂	17.4
	720	An ₁ Ab ₂₆ Or ₇₃	
Spinel	1070	Titanomagnetite	5.3
	920	Titanomagnetite	
Apatite	1030	Ca ₅ (PO ₄) ₃ OH	0.7
	820	Ca ₅ (PO ₄) ₃ OH	
Ilmenite	920	TiO ₂ = 48 wt% FeO _t = 48 wt%	0.9
	720	TiO ₂ = 50 wt% FeO _t = 48 wt%	
Garnet	850	Al ₅₈ Gr ₁₆ Py ₂₆	1.5
	720	Al ₆₇ Gr ₁₅ Py ₁₈	

The total crystallized amount represents ~78 % of the parental magma. At the end of the model (i.e. 720 °C), there is still ~22 % liquid remaining. *Wo* wollastonite, *En* enstatite, *Fs* ferrosilite, *An* anorthite, *Ab* albite, *Or* orthoclase, *Al* almandine, *Gr* grossular, *Py* pyrope

Table 6 Proportion and composition of crystallized minerals in the garnet-suppressed model

Mineral	T (°C)	Composition	Amount crystallized (%)
Orthopyroxene	1170	Wo ₃ En ₇₄ Fs ₂₃	5.0
	1120	Wo ₄ En ₆₉ Fs ₂₇	
Clinopyroxene	1110	Wo ₃₈ En ₄₃ Fs ₁₉	0.3
Pigeonite	1110	Wo ₁₃ En ₅₇ Fs ₃₀	15.4
	720	Wo ₃ En ₂₁ Fs ₇₆	
Plagioclase	1030	An ₄₈ Ab ₄₈ Or ₄	33.6
	720	An ₂₃ Ab ₇₁ Or ₇	
Alkali feldspar	910	An ₄ Ab ₃₄ Or ₆₂	17.2
	720	An ₁ Ab ₂₅ Or ₇₄	
Spinel	1070	Titanomagnetite	5.3
	920	Titanomagnetite	
Apatite	1030	Ca ₅ (PO ₄) ₃ OH	0.7
	820	Ca ₅ (PO ₄) ₃ OH	
Ilmenite	920	TiO ₂ = 48 wt% FeO _t = 48 wt%	0.9
	720	TiO ₂ = 48 wt% FeO _t = 50 wt%	

The total crystallized amount represents ~78 % of the parental magma. At the end of the model (i.e. 720 °C), there is still ~22 % liquid remaining. *Wo* wollastonite, *En* enstatite, *Fs* ferrosilite, *An* anorthite, *Ab* albite, *Or* orthoclase

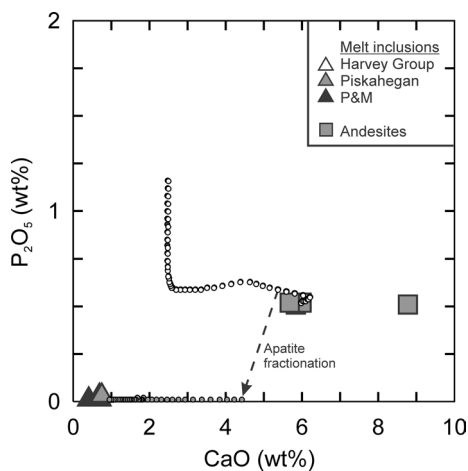


Fig. 14 MELTS modeling for the evolution of CaO and P₂O₅. The overlapping black and white dots represent the liquid evolution compositions of the garnet and garnet-suppressed models based on the starting composition in Table 4. The gray dots are the ‘additional apatite’ fractionation compositions. The modeled composition was adjusted to maintain P₂O₅ at 0.01 wt%. Composition of the apatite from Deer et al. (1992): CaO = 55.84 wt%; P₂O₅ = 42.05 wt%. Additional data from Gray (2010)

The release of magma and fluids from the top of the chamber may produce an ash flow with composition of the Harvey rhyolites. The magma chamber was probably at a mid-crustal depth because felsic magma tends to erupt as ash-flow tuffs and form a caldera from such reservoirs (John 2001). The zoned pyroclastic sequences indicate that the magma chamber of the Mount Pleasant caldera was zoned (McCutcheon et al. 1997). Zoned magma chambers are typically more fertile (i.e., containing ore-forming fluids) than large homogeneous magma chambers (Rytuba 1994).

Uranium mineralization

The Harvey Group, which can be considered to be a part of the Mount Pleasant volcanic caldera complex (McCutcheon et al. 1997; McLeod and Smith 2010), is a promising site for uranium mineralization and represents a potentially important uranium source for a deposit. The group is composed predominantly of highly fractionated peraluminous rhyolitic rocks (ignimbrites, pyroclastics, and lavas). Volcanic rocks are mainly aphyric, and most U was

probably hosted by volcanic glass (e.g., Dostal and Capedri 1975; Dostal et al. 1976; Zielinski 1978, 1981), which has been strongly devitrified by hydrothermal alteration. Glass devitrification facilitates the release of uranium from the rhyolites and is easily leachable by oxidizing hydrothermal fluids. Gray et al. (2011) reported the U contents of silicate melt inclusions trapped in quartz phenocrysts of rhyolite of ~20 ppm. This value is comparable to the U contents of the U-rich Macusani volcanic glass (Pichavant et al. 1988; Nash 2010) and volcanic glass in Transbaikalia, which is considered to represent a U source for the Streltsovskoye deposit (Cuney and Kyser 2015; Chabiron et al. 2003). A comparison of the high U contents and low Th/U ratios of the melt inclusions (~2.3; Gray et al. 2011) with those of the rhyolitic whole rocks of the Harvey Group (Fig. 10) indicates that a significant amount of the initial U from the rhyolite has been lost during the alteration processes. Thus, the Harvey rocks represent a potential source of U via devitrification of the glass by oxidizing fluids. This process could have produced strata-bound vein-type mineralization hosted in volcanic rocks and associated sediments.

Conclusions

The 360 Ma old volcanic rocks of the Harvey Group are highly fractionated peraluminous within-plate F-rich rhyolites. Compared to typical peraluminous rhyolites or granites (e.g., Clarke 1992), the rocks, including the melt inclusions, have higher Rb, Th, U, Y and heavy REE, but lower contents of CaO, MgO, P₂O₅, TiO₂, Ba, Sr and Eu and have uncommon distributions of REE and HFSE. The rhyolites were formed by fractional crystallization of an intermediate magma similar to andesites of the Mount Pleasant caldera complex. The highly evolved Harvey melts enriched in several lithophile elements formed at the top of felsic magma chamber where also volatile elements (F, Cl, water) became concentrated. Although topaz has not been found in the Harvey volcanics, their major and trace element compositions resemble topaz-bearing rhyolites which are known to host U mineralization. The volcanic rocks of the Piskahegan and Harvey groups have similar Nd isotopic characteristics and could have been formed in the same magma chamber. However, unlike the Harvey rocks, the Piskahegan rhyolites were not generated at its apex. The Harvey volcanic rocks had the potential to develop a significant mineralization of U. The erupted U-rich glassy rhyolites may be favorable U source rock amendable to leaching by post-magmatic hydrothermal and meteoric water. The bulk of U in these rocks resides in glass and accessory minerals. During the secondary processes, glass was devitrified and its U was removed either by hydrothermal or meteoric

water and deposited in mineralized zones. The Harvey part of the caldera complex composed of highly fractionated pyroclastic rhyolitic material represents a promising setting for the genesis of U deposits related to volcanic rocks.

Acknowledgments We gratefully acknowledge funding for this project through the grants of the New Brunswick Department of Energy and Mines, Geological Surveys Branch and the Natural Sciences and Engineering Research Council of Canada (Discovery grants to J.D. and J.H.). Constructive reviews by two anonymous referees improved the manuscript. We thank Malcom McLeod for the initiation of this project and numerous constructive discussions, Randy Corney for technical assistance and Andrew MacRae for taking a field photo.

References

- Abdel-Rahman AM (2006) Petrogenesis of anorogenic peralkaline granitic complexes from eastern Egypt. *Miner Mag* 70:27–50
- Anderson HE (1992) A chemical and isotopic study of the age, petrogenesis and magmatic evolution of the Mount Pleasant caldera complex, New Brunswick. PhD thesis, Carleton University, Ottawa, Ontario
- Andersen T (2002) Correction of common lead in U-Pb analyses that do not report ²⁰⁴Pb. *Chem Geol* 192:59–79
- Bau M (1996) Controls on the fractionation of isovalent trace elements in magmatic and aqueous systems: evidence from Y/Ho, Zr/Hf and lanthanide tetrad effects. *Contrib Mineral Petrol* 123:323–333
- Beaudin J, LeGallais C, Schimann K (1980) Rapport final des travaux de la campagne 1979: Groupe de claims Manners Sutton, Project 24–147, Comte York, Nouveau-Brunswick, vol 1, p 152
- Benjamin ER, Plank T, Wade JA, Kelley KA, Hauri EH, Alvarado GE (2007) High water contents in basaltic magmas from Irazu Volcano, Costa Rica. *J Volcanol Geother Res* 168:68–92
- Bouvier A, Vervoort JD, Patchett PJ (2008) The Lu-Hf and Sm-Nd isotopic composition of CHUR: constraints from unequilibrated chondrites and implications for the bulk composition of terrestrial planets. *Earth Planet Sci Lett* 273:48–57
- Capella Resources Ltd. (2007) Harvey project: Harvey Project assay highlights. <http://www.capellaresources.com/s/HarveyProject.asp>
- Castor SB, Henry CD (2000) Geology, geochemistry, and origin of volcanic rock-hosted uranium deposits in northwestern Nevada and southeastern Oregon, US. *Ore Geol Rev* 16:1–40
- Cerny P, Blevin PL, Cuney M, London D (2005) Granite-related ore deposits. *Econ Geol* 100:337–370
- Chabiron A, Cuney M, Poty B (2003) Possible uranium sources for the largest uranium district associated with volcanism: the Streltsovka caldera (Transbaikalia, Russia). *Miner Depos* 38:127–140
- Chayes F (1985) IGBADAT: a world data base for igneous petrology. *Episodes* 8:245–251
- Chiu HY, Chung SL, Wu FY, Liu D, Liang YH, Lin IJ, Iizuka Y, Xie LW, Wang Y, Chu MF (2009) Zircon U-Pb and Hf isotopic constraints from eastern Transhimalayan batholiths on the precollisional magmatic and tectonic evolution in southern Tibet. *Tectonophysics* 477:3–19
- Christiansen EH, Bikun JV, Sheridan MF, Burt DM (1984) Geochemical evolution of topaz rhyolites from the Thomas Range and Spor Mountain, Utah. *Am Miner* 69:223–236
- Christiansen EH, Sheridan MF, Burt DM (1986) The geology and geochemistry of Cenozoic topaz rhyolites from the western United States. *Geol Soc Am Spec Pap* 205:1–82
- Christiansen EH, Kowallis BJ, Dorais MJ, Hart GL, Mills CN, Pickard M, Parks E (2015) The record of volcanism in the Brushy

- Basin Member of the Morrison Formation: implications for the Late Jurassic of western North America. *Geol Soc Am Spec Pap* 513:399–439
- Clarke DB (1992) *Granitoid rocks*. Chapman & Hall, London
- Cuney M, Kyser TK (2015) Geology and geochemistry of uranium and thorium deposits. *Miner Assoc Can Short Course* 46:345
- Deer WA, Howie RA, Zussman J (1992) *An introduction to the rock forming minerals*, 2nd edn. Addison Wesley Longman, Essex, p 696
- DePaolo DJ (1988) Neodymium isotope geochemistry: an introduction. Springer, New York
- Dostal J, Capedri S (1975) Partition coefficients of uranium for some rock-forming minerals. *Chem Geol* 15:285–294
- Dostal J, Capedri S (1978) Uranium in metamorphic rocks. *Contrib Miner Petrol* 66:409–414
- Dostal J, Chatterjee AK (1995) Origin of topaz-bearing and related peraluminous granites of late Devonian Davis Lake pluton, Nova Scotia, Canada. *Chem Geol* 123:67–88
- Dostal J, Capedri S, Dupuy C (1976) Uranium and potassium in calc-alkaline volcanic rocks from Sardinia. *Lithos* 9:179–183
- Dostal J, Wilson RA, Keppie JD (1989) Geochemistry of Siluro-Devonian Tobique volcanic belt in northern and central New Brunswick (Canada): tectonic implications. *Can J Earth Sci* 26:1282–1296
- Dostal J, Chatterjee AK, Kontak DJ (2004) Chemical and isotopic (Pb, Sr) zonation in a peraluminous granite pluton: role of fluid fractionation. *Contrib Miner Petrol* 147:74–90
- Dostal J, Kontak DJ, Karl SM (2014) The Early Jurassic Bokan Mountain peralkaline granitic complex (southeastern Alaska): geochemistry, petrogenesis and rare metal-mineralization. *Lithos* 202–203:395–412
- Dostal J, Keppie JD, Wilson RA (2016) Nd isotopic and trace element constraints on the source of Silurian–Devonian mafic lavas in the Chaleur Bay Synclinorium of New Brunswick (Canada): tectonic implications. *Tectonophys*. doi:10.1016/j.tecto.2015.10.002
- Duc-Tin Q, Keppler H (2015) Monazite and xenotime solubility in granitic melts and the origin of the lanthanide tetrad effect. *Contrib Miner Petrol* 169:8. doi:10.1007/s00410-014-1100-9
- Dunning GR, Barr SM, Giles PS, McGregor DC, Pe-Piper G, Piper DJW (2002) Chronology of Devonian to early Carboniferous rifting and igneous activity in southern Magdalen Basin based on U-Pb (zircon) dating. *Can J Earth Sci* 39:1219–1237
- Fujimaki H (1986) Partition-coefficients of Hf, Zr, and REE between zircon, apatite, and liquid. *Contrib Miner Petrol* 94:42–45
- Ghiorso MS, Sack RO (1995) Chemical mass transfer in magmatic processes IV. A revised and internally consistent thermodynamic model for the interpolation and extrapolation of liquid-solid equilibria in magmatic systems at elevated temperatures and pressures. *Contrib Miner Petrol* 119:197–212
- Gibling MR, Culshaw N, Rygel MC, Pasucci V (2009) The Maritimes Basin of Atlantic Canada: Basin creation and destruction in the collision zone of Pangea. *Sediment Basins World* 5:211–238
- Gray TR (2010) Late Paleozoic felsic volcanics in southern New Brunswick and related uranium mineralization. MSc thesis, Saint Mary's University, Halifax, Nova Scotia
- Gray TR, Hanley JJ, Dostal J, Guillong M (2011) Magmatic enrichment of uranium, thorium and rare earth elements in late Paleozoic rhyolites of southern New Brunswick, Canada: evidence from silicate melt inclusions. *Econ Geol* 106:127–143
- Griffin WL, Pearson NJ, Belousova E, Jackson SE, van Acherberg E, O'Reilly SY, Shee SR (2000) The Hf isotope composition of cratonic mantle: LAM–MC–ICPMS analysis of zircon megacrysts in kimberlites. *Geochim Cosmochim Acta* 64:133–147
- Griffin WL, Pearson NJ, Belousova EA, Saeed A (2006) Comment: Hf-isotope in zircon 91500. *Chem Geol* 233:358–363
- Hassan HH, Hale WE (1988) Uraniferous granite and rhyolite of Devonian–Carboniferous age in southwestern New Brunswick, Canada. *Uranium* 4:245–259
- Hildreth WS, Wilson CJN (2007) Compositional zoning in the Bishop Tuff. *J Petrol* 48:951–999
- IAEA (International Atomic Energy Agency) (2009) World distribution of uranium deposits (UDEPO) with uranium deposit classification. Vienna, Austria
- Irber W (1999) The lanthanide tetrad effect and its correlation with K/Rb, Eu/Eu*, Sr/Eu, Y/Ho and Zr/Hf of evolving peraluminous granite suites. *Geochim Cosmochim Acta* 63:489–508
- Jahn BM, Wu FY, Capdevila R, Martineau F, Wang YX, Zhao ZH (2001) Highly evolved juvenile granites with tetrad REE patterns: the Woduhe and Baerzhe granites from the Great Xing'an (Khangai) Mountains in NE China. *Lithos* 59:171–198
- John DA (2001) Miocene and early Pliocene epithermal gold–silver deposits in the northern Great Basin, Western United States—characteristics, distribution, and relationship to magmatism. *Econ Geol* 96:1827–1853
- Keppie JD, Dostal J, Murphy JB, Cousens BL (1997) Palaeozoic within-plate volcanic rocks in Nova Scotia (Canada) reinterpretation: isotopic constraints on magmatic source and palaeocontinental reconstructions. *Geol Mag* 134:425–447
- Keppie JD, Murphy JB, Nance RD, Dostal J (2012) Mesoproterozoic Oaxaquia-type basement in peri-Gondwanan terranes of Mexico, the Appalachians and Europe: TDM age constraints on extent and significance. *Intern Geol Rev* 54:313–324. doi:10.1080/00206814.2010.543783
- Le Maitre RW et al (1989) *Igneous rocks: a classification glossary of terms*. Cambridge University Press, Cambridge
- Linnen RL, Cuney M (2005) Granite-related rare-element deposits and experimental constraints on Ta-Nb-W-Sn-Zr-Hf mineralization. In: Linnen RL, Samson IM (eds) *Rare-element geochemistry and mineral deposits*. *Geol Assoc Canada Short Course*, vol 17, pp 45–68
- Ludwig KR (2001) *Isoplot/Ex rev. 2.49*. A geochronological toolkit for Microsoft Excel. Berkeley Geochronology Center, Special Publication No. 1a, p 55
- Marks M, Markl G (2001) Fractionation and assimilation processes in the alkaline augite syenite unit of the Ilímaussaq intrusion, South Greenland, as deduced from phase equilibria. *J Petrol* 42:1947–1969
- McCutcheon SR, Anderson HE, Robinson PT (1997) Stratigraphy and eruptive history of the Late Devonian Mount Pleasant Caldera Complex, Canadian Appalachians. *Geol Mag* 134:17–36
- McLeod M, Johnson S (2007) Exploration activity and setting of uranium in New Brunswick: Québec Exploration, Chateau Frontenac, 26–29 November 2007. http://www.quebecexploration.qc.ca/2007/pdf/session_05/S5-08_mcleod.pdf
- McLeod MJ, Smith EA (2010) Uranium. New Brunswick Department of Natural Resources; Lands, Minerals and Petroleum Division, Mineral Commodity Profile No. 6, p 7
- Monecke T, Kempe U, Monecke J, Sala M, Wolf D (2002) Tetrad effect in rare earth element distribution patterns: a method of quantification with application to rock and mineral samples from granite-related rare metal deposits. *Geochim Cosmochim Acta* 66:1185–1196
- Moore G, Carmichael ISE (1998) The hydrous phase equilibria (to 3 kbar) of an andesite and basaltic andesite from western Mexico: constraints on water content and conditions of phenocryst growth. *Contrib Miner Petrol* 130:304–319
- Murphy JB, Dostal J, Keppie JD (2008) Neoproterozoic–Early Devonian magmatism in the Antigonish Highlands, Avalon terrane, Nova Scotia: tracking the evolution of the mantle and crustal sources during the evolution of the Rheic Ocean. *Tectonophys* 461:181–201

- Murphy JB, Dostal J, Gutierrez-Alonso G, Keppie JD (2011) Early Jurassic magmatism on the northern margin of CAMP: derivation from a Proterozoic sub-continental lithospheric mantle. *Lithos* 123:158–164
- Nash JT (2010) Volcanogenic uranium deposits—Geology, geochemical processes, and criteria for resource assessment: US Geological Survey Open-File Report 2010-1001, p 99
- Osborn EF (1959) Role of oxygen pressure in the crystallization and differentiation of basaltic magma. *Am J Sci* 257:609–647
- Payette C, Martin RF (1986a) The Harvey volcanic suite in New Brunswick: I: Inclusions of magma in quartz phenocrysts. *Can Miner* 24:557–570
- Payette C, Martin RF (1986b) The Harvey volcanic suite in New Brunswick: II: Postmagmatic adjustments in the mineralogy and bulk composition of high fluorine rhyolite. *Can Miner* 24:571–584
- Pearce JA, Harris NBW, Tindle AG (1984) Trace element discrimination diagrams for tectonic interpretation of granitic rocks. *J Petrol* 25:956–983
- Pe-Piper G, Piper DJW (1998) Geochemical evolution of Devonian–Carboniferous igneous rocks of the Magdalen Basin, Eastern Canada: Pb- and Nd-isotope evidence for mantle and lower crustal sources. *Can J Earth Sci* 35:201–221
- Pichavant M, Kontak DJ, Herrera JV, Clark AH (1988) The Miocene–Pliocene Macusani volcanics, SE Peru. *Contrib Miner Petrol* 100:300–324
- Rudnick RL, Gao S (2003) Composition of the continental crust. In: Rudnick RL (ed) *The crust*, vol 3. Elsevier, London, pp 1–64
- Rytuba JJ (1994) Evolution of volcanic and tectonic features in caldera settings and their importance in the localization of ore deposits. *Econ Geol* 89:1687–1696
- Scherer E, Munker C, Mezger K (2001) Calibration of the lutetium–hafnium clock. *Science* 293:683–687
- Shaw DM, Dostal J, Keays RR (1976) Additional estimates of continental surface Precambrian Shield composition in Canada. *Geochim Cosmochim Acta* 40:73–83
- Sinclair WD, Kooiman GJA, Martin DA, Kjarsgaard IM (2006) Geology, geochemistry and mineralogy of indium resources at Mount Pleasant, New Brunswick, Canada. *Ore Geol Reviews* 28:123–145
- Sisson TW, Ratajevski K, Hankins WB, Glazner AF (2005) Voluminous granitic magmas from common basaltic source. *Contrib Miner Petrol* 148:635–661
- Smith PM, Asimow PD (2005) *Adiabat_1ph*: a new public front-end to the MELTS, pMELTS, and pHMELTS models. *Geochim Geophys Geosyst* 6:Q02004. doi:10.1029/2004GC000816
- Stepanov AS, Hermann J, Rubatto D, Rapp RP (2012) Experimental study of monazite/melt partitioning with implications for the REE, Th and U geochemistry of crustal rocks. *Chem Geol* 300–301:200–220
- Sun SS, McDonough W F (1989) Chemical and isotopic systematics of oceanic basalts: implications for mantle composition and processes. In: Saunders AD, Norry MJ (eds) *Magmatism in the Ocean Basins*. *Geol Soc London Spec Pub*, vol 42, pp 313–345
- Tanaka T et al (2000) JNd-1: a Neodymium isotopic reference in consistency with La Jolla Neodymium. *Chem Geol* 168:279–281
- Taylor RP (1992) Petrological and geochemical characteristics of the Pleasant Ridge zinnwaldite-topaz granite, southern New Brunswick, and comparison with other topaz-bearing felsic rocks. *Can Miner* 30:895–921
- Thorne KG, Fyffe LR, Creaser RA (2013) Re–Os geochronological constraints on the mineralizing events within the Mount Pleasant Caldera: implications for the timing of subvolcanic magmatism. *Atl Geol* 49:131–150
- Tucker RD, Bradley DC, Straeten CA, Harris AG, Ebert JR, McCutcheon SR (1998) New U–Pb zircon ages and the duration and division of Devonian time. *Earth Planet Sci Lett* 158:175–186
- Turner SP, Foden JD, Morrison RS (1992) Derivation of some A-type magmas by fractionation of basaltic magma: an example from the Padthaway Ridge, South Australia. *Lithos* 28:151–179
- Van Staal CR, Barr SM, Murphy JB (2012) Provenance and tectonic evolution of Ganderia: constraints on the evolution of the Iapetus and Rheic oceans. *Geology* 40:987–990
- Veksler IV, Dorfman AM, Kamenetsky M, Dulski P, Dingwell DB (2005) Partitioning of lanthanides and Y between immiscible silicate and fluoride melts, fluorite and cryolite and the origin of the lanthanide tetrad effect in igneous rocks. *Geochim Cosmochim Acta* 69:2847–2860
- Whalen JB, Fyffe LR, Longstaffe FJ, Jenner GA (1996) The position and nature of the boundary, southern New Brunswick, based on geochemical and isotopic data from granitoid rocks. *Can J Earth Sci* 33:129–139
- Wiedenbeck M, Allé P, Corfu F, Griffin WL, Meier M, Oberli F, Von Quadt A, Roddick JC, Spiegel W (1995) Three natural zircon standards for U–Th–Pb, Lu–Hf, trace element and REE analyses. *Geostand Newsl* 19:1–23
- Winchester JA, Floyd PA (1977) Geochemical discrimination of different magma series and their differentiation products using immobile elements. *Chem Geol* 20:325–343
- Winter JD (2001) *An introduction to igneous and metamorphic petrology*. Prentice Hall, New Jersey
- Woodhead JD, Hergt JM (2005) A preliminary appraisal of seven natural zircon reference materials for in situ Hf isotope determination. *Geostand Geoanalytical Res* 29:183–195
- Yang XM, Lentz RL, McCutcheon SR (2003) Petrochemical evolution of subvolcanic granitoid intrusions within the Late Devonian Mount Pleasant Caldera, southwestern New Brunswick, Canada: comparison of Au versus Sn–W–Mo–polymetallic mineralization systems. *Atl Geol* 39:97–121
- Yurimoto H, Duke EF, Papike JJ, Shearer CK (1990) Are discontinuous chondrite-normalized REE patterns in pegmatitic granite systems the result of monazite fractionation? *Geochim Cosmochim Acta* 54:2141–2145
- Zielinski RA (1978) Uranium abundances and distribution in associated glassy and crystalline rhyolites of the western United States. *Geol Soc Am Bull* 89:409–414
- Zielinski RA (1981) Experimental leaching of volcanic glass—Implications for evaluation of glassy volcanic rocks as sources of uranium. In: Goodell PC, Waters AC (eds) *Uranium in volcanic and volcanoclastic rocks*. American Association of Petroleum Geologists Studies in Geology, vol 13, pp 1–11
- Zimmer MM, Plank T, Hauri EH, Yogodzinski GM, Stealing P, Larsen J, Singer B, Jicha B, Mandeville C, Nye C (2010) The role of water in generating the calc-alkaline trend: new volatile data for Aleutian magmas and a new tholeiitic index. *J Petrol* 51:2411–2444